

We are IntechOpen, the world's leading publisher of Open Access books Built by scientists, for scientists

6,900

Open access books available

186,000

International authors and editors

200M

Downloads

Our authors are among the

154

Countries delivered to

TOP 1%

most cited scientists

12.2%

Contributors from top 500 universities



WEB OF SCIENCE™

Selection of our books indexed in the Book Citation Index
in Web of Science™ Core Collection (BKCI)

Interested in publishing with us?
Contact book.department@intechopen.com

Numbers displayed above are based on latest data collected.
For more information visit www.intechopen.com



Nonlinear Optoelectronic Devices Based on Nanocrystalline Silicon Films: Acoustoelectrical Switchers for Optical Modes, Nonlinear Optical Switchers and Lasers

Dmitry E. Milovzorov
*FLUENS TECHNOLOGY GROUP, LTD, Moscow
Russia*

1. Introduction

Since 2000, the nanostructured materials have received a great application in optoelectronic devices development. Nanocrystalline silicon films are used now as for performing the new memory devices as to make thin film transistors for displays. Optical switches are used already two decades in optical communication systems. The switching times were varied from μs to ns. However, the possible increasing the rate of switching can be results in new optical computer creation the main principal of which are based on nonlinear switches. Accordingly, the high degree of integration of elements is, also, very attractive. Because, the miniaturization of switch is significant.

This investigation is devoted to possible nonlinear switch design the main principle of which is based on the control of the nonlinear-optical response enhancement for nanostructured silicon films by applying external electrical field. First, it is discussed a suitable nonlinear optical system based on various types of silicon films: amorphous, nanocrystalline and polycrystalline (D. Milovzorov et al., 1998, 1999, 2001). Also, each silicon film differs from the other in crystal phase fraction, size distribution of nanocrystals, their crystal orientation, by various types of chemical bonding and defects, their densities, and density and sizes of nanoscale holes. The next type of proposed devices is acoustoelectrical switches for optical modes inside the laser cavity. Acoustoelectric effect was detected in various materials such as n-type germanium (Weinreich et al., 1959), GaAs/LiNbO₃ structure (Rotter et al., 1998). In present work the acoustoelectrical effect is studied in nanostructural silicon thin films by applied external electric field due to their specific structural and chemical properties. The third type of optoelectronic devices is lasers based on silicon films such as Raman laser and laser with nonlinear two-photon resonant pumping. The new electronic devices based on natural luminescent and nonlinear properties of oxidized nanocrystalline silicon film can be easily resolved numerous problems of communications and computing by using combination of new spectral lines in IR, visible and UV ranges. Theoretical approach assists to find the main mechanisms of evolution of inverted population and appearance of laser generation modes.

2. Acoustoelectric effects by Raman scattering

2.1 Raman scattering from silicon films

The Raman spectra for poly-Si films consist of a narrow line near 520 cm⁻¹ arising from a crystalline phase and a broad line around 480 cm⁻¹ from an amorphous phase. The ρ value was estimated from the ratio of the Raman integrated intensity for the crystalline component to the total intensity, using the ratio of the integrated Raman cross-section for the crystalline phase to that for an amorphous phase. The random silicon network Gauss-distributed in their bond lengths with various deviations, and phonon wave numbers is spread. The regular bonding network has the Lorentz shape of its spectral line. Our possible interpretation of a-Si Raman spectra decomposition is a possible recognition the role of point defects and inserted impurities which cause the changes in structural properties of film. It is assumed, that the a-Si film with high density of defects such as silicon vacancies causes the spectral peak around 465 cm⁻¹, but after annealing there is a spectral shift in wavenumber 465 cm⁻¹ → 475 cm⁻¹. By hydrogen dilution of gas mixture by PECVD of a-Si the Raman peak position is changed from 475 cm⁻¹ to the 480 cm⁻¹ (D.V.Tsu et al., 2001). It is supposed, that the Raman data of hydrogenised amorphous silicon film result in the spectral peak around 45-447 cm⁻¹ (D. Han et al., 2000) corresponds the LO mode, but the 480 cm⁻¹ for TO mode. For the higher structural relaxed silicon thin film by high level of hydrogen dilution the TO mode reflects in 490 cm⁻¹ value of peak position. The spectral peak width changed from the value of 40 cm⁻¹ for a-Si to the 70 cm⁻¹ for a-Si:H.

There are many interpretations of Raman spectral data concerning the optical response from crystalline silicon phase around 520 cm⁻¹, various kinds of intermediate, μ c-Si or nc-Si, or grain boundary response around 494-501 cm⁻¹, and amorphous silicon phase at the wave number value of 480 cm⁻¹, (D. Han et al., 2003). Figure 1 shows the various types of decompositions of Raman spectrum for microcrystalline silicon film with thickness around 100 nm. This film was deposited at 380 °C. By using this procedure we use three or four peaks approximations. Figure 1 a illustrates the three peak decomposition with c-Si related spectral line around 520 cm⁻¹, nanocrystalline or intermediate spectral line in range 500-510 cm⁻¹ and for amorphous silicon is 480 cm⁻¹. The next Fig. 1 b shows the Raman data with noise signal for comparison and fourth spectral component (~490 cm⁻¹) is related to hydrogenated amorphous silicon network. According to the Matsuda work (Matsuda, 1999, 2004) it is possible to deposit the μ c-Si:H film with low content of P_b defects at relatively low temperatures 200-300°C. By these temperature conditions the hydrogen diffusion is effective compare to the diffusion rates of SiH₃ and SiH₂ radicals. The hydrogen terminates all the dangling bonds. The defects levels spectral intensity of Raman spectra becomes lower. The spectral characteristics of amorphous-related peaks are changed by the hydrogen saturation of dangling bonds.

2.2 Raman spectroscopy from thin crystalline silicon films on glass substrate

For additional confirmation the nature of optical response from silicon thin film we tried to carry on the analysis the Stocks components of Raman scattering spectral lines and physics of laser light absorption by surface layer. Absorption of radiation by c-Si film on glass substrate can be written as: $I = I_0 \exp(-\alpha Z_{c-Si}) \exp(-\beta Z_{glass})$.

The spectral intensity of radiation by Raman Scattering can be distinguished as following:

$$I^{Scattered} = \int_{\omega_1}^{\omega_2} I_{c-Si}^{Scattered}(\omega) d\omega + \int_{\omega_3}^{\omega_4} I_{glass}^{Scattered}(\omega) d\omega. \quad (1)$$

The energy of radiation can be expressed as addition of energies of all dipoles:

$$\int I_{c-Si}^{Scattered}(\omega) d\omega \cong \eta Z_{c-Si} d \sqrt{I_0}.$$

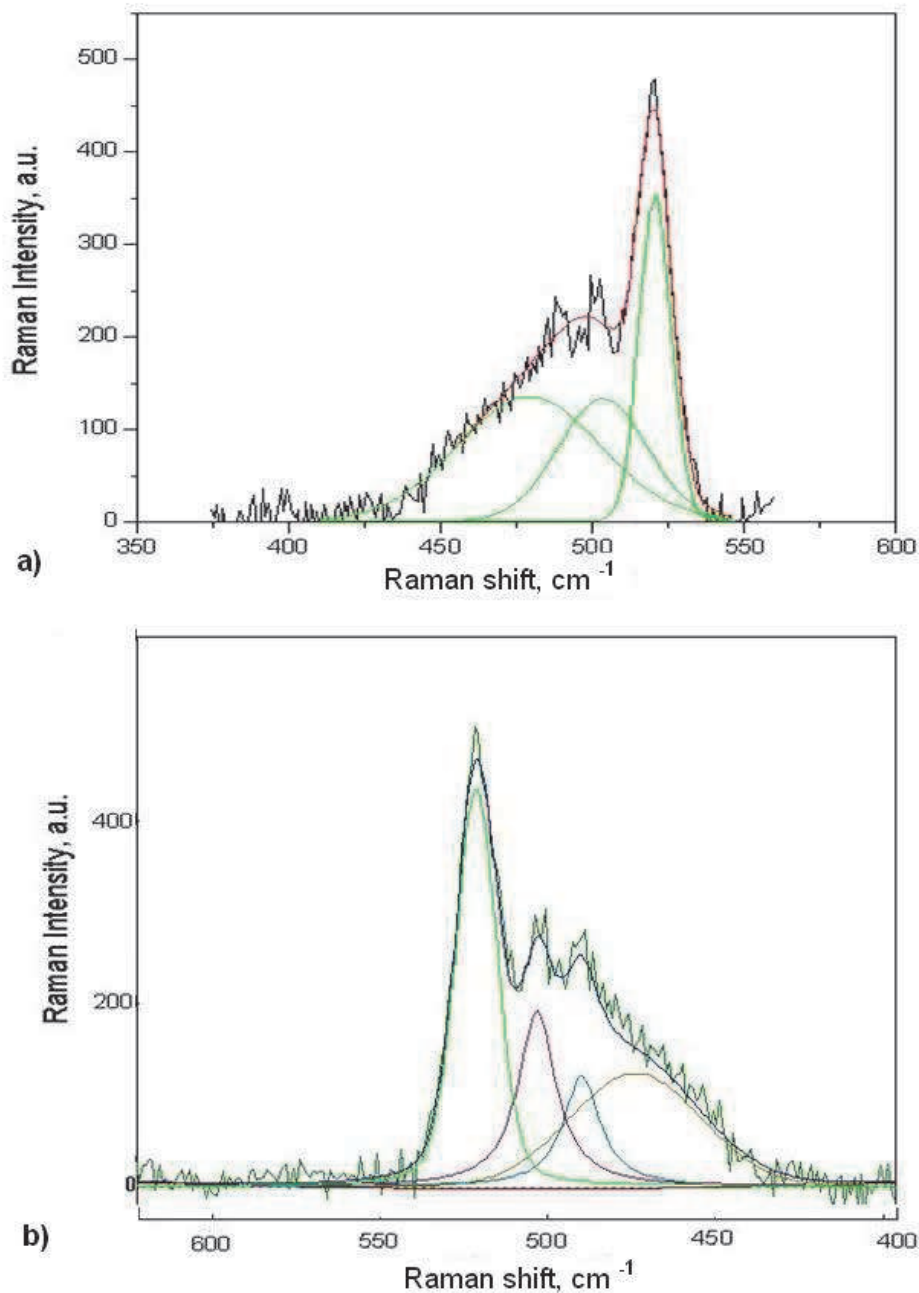


Fig. 1. Raman spectra deconvolution by using a) 3 peaks approximation: c-Si, for 520 cm⁻¹; a-Si for 480 cm⁻¹ and intermediate or nanocrystalline for 500-510 cm⁻¹; b) 4 peaks approximation: for c-Si (520 cm⁻¹); a-Si (480 cm⁻¹); nanocrystalline (500-510 cm⁻¹) and hydrogenated a-Si:H for 490cm⁻¹.

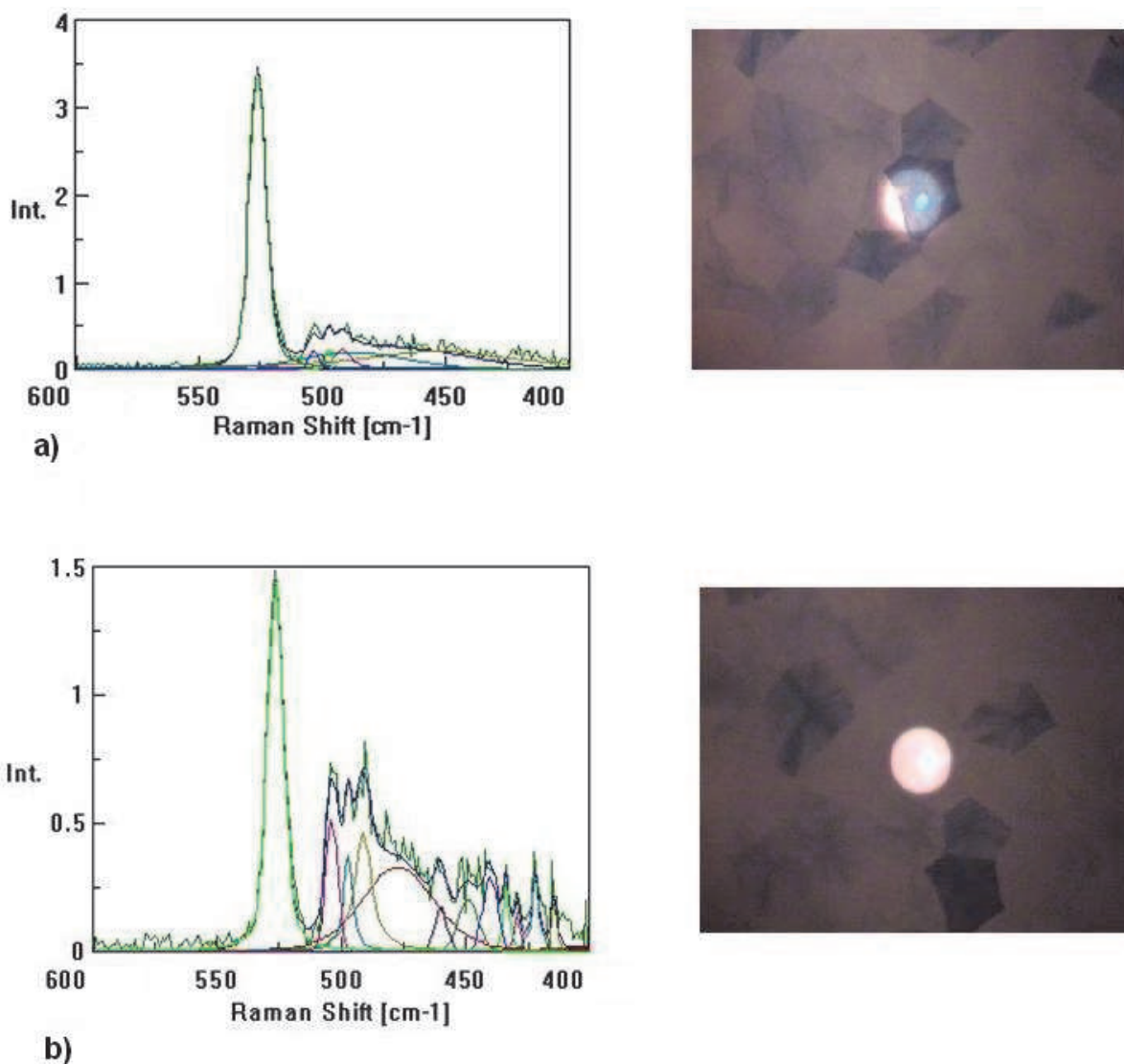


Fig. 2. Raman spectra and micro photo of Secco etched silicon film with thickness of film is around 25 nm -a); Raman spectra micro photo of Secco etched silicon film with thickness of film is around 17 nm- b).

We assume that the D is a laser beam diameter and the density of dipoles can be written as following:

$$N_{Si} = \frac{1}{4} \pi D^2 Z_{c-Si} \quad (2)$$

The thin film thickness can be estimate by using Raman scattering signal from standard film sample and suggested that silicon film is fully crystallized: $Z_{1;c-Si} = Z_{c-Si} \rho$.

For the real thickness of fully crystallized silicon (see Fig. 2) film $Z=50$ nm, we can estimate the thickness of etched silicon film as ratio between peaks' squares under crystalline phase around 520 cm^{-1} and amorphous phase around 480 cm^{-1} multiplied on 50 nm. For the thin film on Fig. 3 it is seen that the thickness value is around 25 nm. By Secco etching of Si film the rate of etching is around 3-4 nm/s. According to our estimations, the thickness of thin silicon film shown on Fig. 2.4 is equal to 17 nm.

2.3 Raman scattering from multicomponent silicon films

Figure 3 shows the Raman spectra porous silicon film on the Corning 7059 (Fig.3 a) glass substrate, Raman map of film's area $9\mu\text{m} \times 9\mu\text{m}$ (see Fig.3b), the scheme of silicon film structure (Fig. 3c) and its atomic-force microscopic (AFM) photo on the area $1\mu\text{m}^2$ (Fig. 3d). It is seen, that crystal phase volume fraction can be estimated by using the Raman

spectroscopy data according to following formula: $\rho = \frac{I_C + I_{nc}}{I_C + I_{nc} + I_A}$, where the values I_C , I_A ,

I_{nc} are intensities of spectral signal on 520 cm^{-1} , 480 cm^{-1} , and $500\text{-}510\text{ cm}^{-1}$, respectively. The ρ value is more than 70% for the silicon films that were shown on Fig.3. Figure 4 illustrates the optical and structural properties of silicon films with nanocrystals included into silicon oxide material and their photo detected by means of AFM. It is clear, that the ρ value is lower for such type of silicon films than mentioned above. It is in the range of 30-50%. However, it is seen the rectangular shape of large (around several hundreds nm) crystals which are made due to low temperatures of deposition and high degree of hydrogen dilution. Also, it is important to note about low pressure and low flow rates of gases.

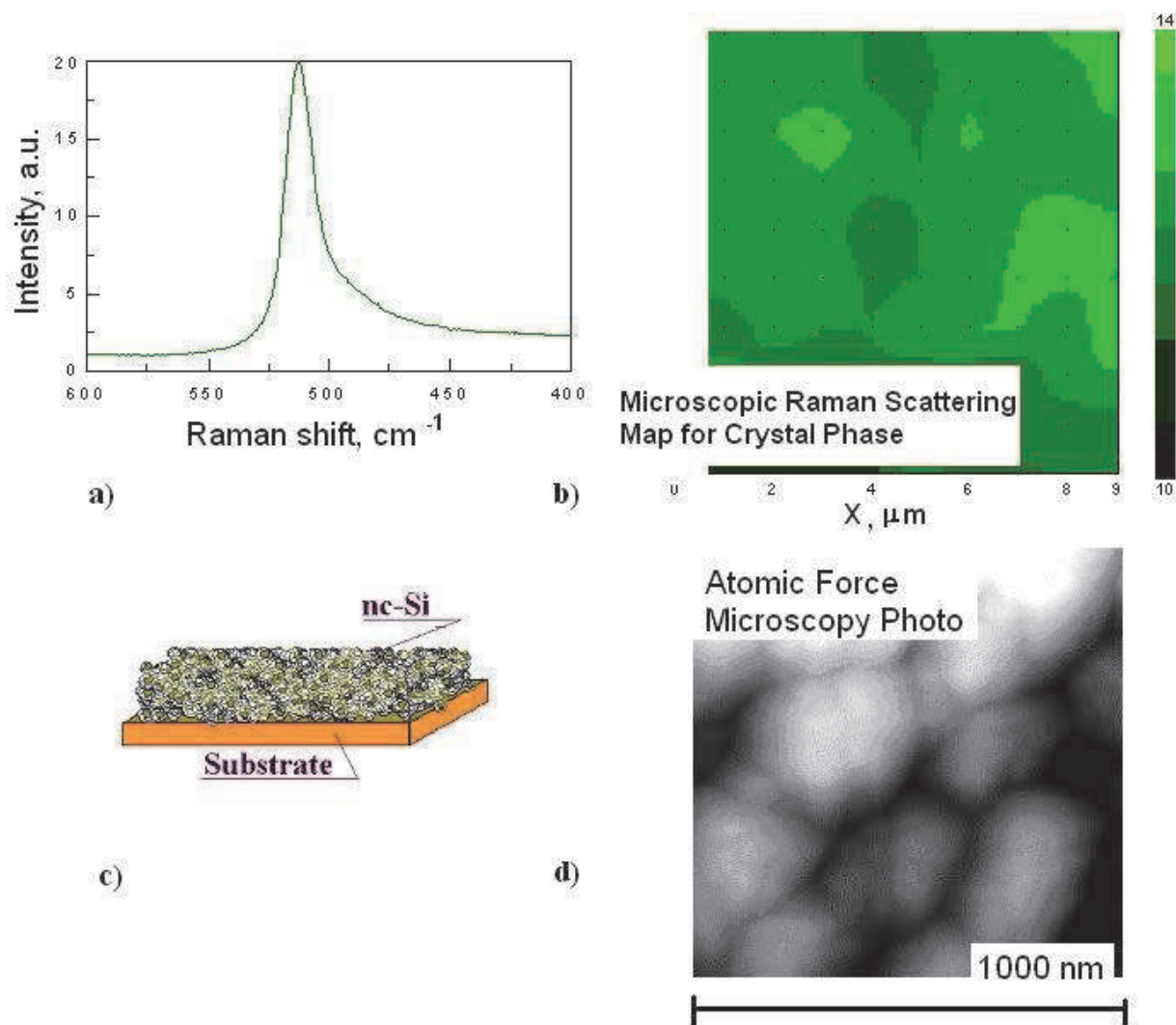


Fig. 3. Raman spectrum -a); and Raman map of crystallized silicon in film on glass substrate -b); scheme of material -c); and its atomic-force microscopic (AFM) photo -d).

The silicon bonding is estimated by using Raman scattering measurements from the ratio:

$$\rho = \frac{\int_0^{\infty} I_{Si}(\omega) d\omega}{\int_0^{\infty} I_{Raman}(\omega) d\omega} \quad (3)$$

The ρ value was estimated from the ratio of the Raman integrated intensity for the silicon-related components to the total intensity, using the ratio of the integrated Raman cross-section for them. The local factor is given by

$$L(\omega, \rho) = \frac{\rho}{4\pi} \frac{(\epsilon_{Si}(\omega) - \epsilon_{SiO_2}(\omega))}{1 + (\epsilon_{Si}(\omega) - \epsilon_{SiO_2}(\omega))(\Lambda - \beta\rho)} \quad (4)$$

where the $\epsilon_{Si}(\omega)$ and ϵ_{SiO_2} are the dielectric functions of silicon and SiO_2 , Λ is the depolarization factor (for sphere is 1/3), β is the Lorentz constant ($\beta=1/3$ for a homogeneous spherical surrounding). The natural Raman spectral width for Gaussian distributed crystallites in their sizes in film depends on the dispersion of phonon wave vector: $\Delta q = 4\pi\sigma/(\delta^2 - \sigma^2)$, where the value of σ is equal to $\max(\epsilon, \theta)$, ϵ is a dispersion of spatial crystallites distribution ($\epsilon = \int f(\delta)\delta^2 d\delta$, $f(\delta)$ is Gaussian distribution function), θ^* is random shape distortion of crystallites from spherical shape $\delta^* = \delta\theta$, where δ^* is random Gaussian distributed value of size of crystallite with random spherical shape, $\langle \delta^* \rangle = \delta \langle \theta \rangle$. The value of θ^* is equal to $\delta(\theta-1)$.

2.4 Laser picosecond spectroscopy

A mode-locked YAG:Nd³⁺ laser radiation with wavelength 532 nm was used as an optical pump of media, but the second-harmonic radiation ($\lambda=1064$ nm) was used for probing of sample's surface. The pulse duration was 120 ps. The pulse repetition rate was 100 MHz and frequency of Q-switched modulation of second-harmonic radiation was 6.2 MHz. The correlation function of reflected signal intensity of probe laser beam was detected by means of pump-probe laser scheme

$$G(t) = \langle I(t)I(t+\tau) \rangle = \frac{1}{T} \int_0^T I(t)I(t+\tau) dt; \quad (5)$$

where $G(t)$ is averaged correlation function, T is the time of detection. It is estimated, that $\Delta\omega$ is a width of level that equals to 12 μ eV for silicon film with $\langle \delta \rangle = 8.5$ nm, and 16 μ eV for silicon film with $\langle \delta \rangle = 14.7$ nm (see Fig. 5 a, upper and down graphs). The most important fact is appearance of quantum beats, which reflect the optical response from two-neighbor level. We suppose that the different fractions of oxygen incorporation in silicon film cause the appearance of neighbor levels inside the band gap with the spectral width (Milovzorov, 2001):

$$\Delta_d = \frac{20\epsilon_x h^3}{m^2 e^2} N_{Si-O} \quad (6)$$

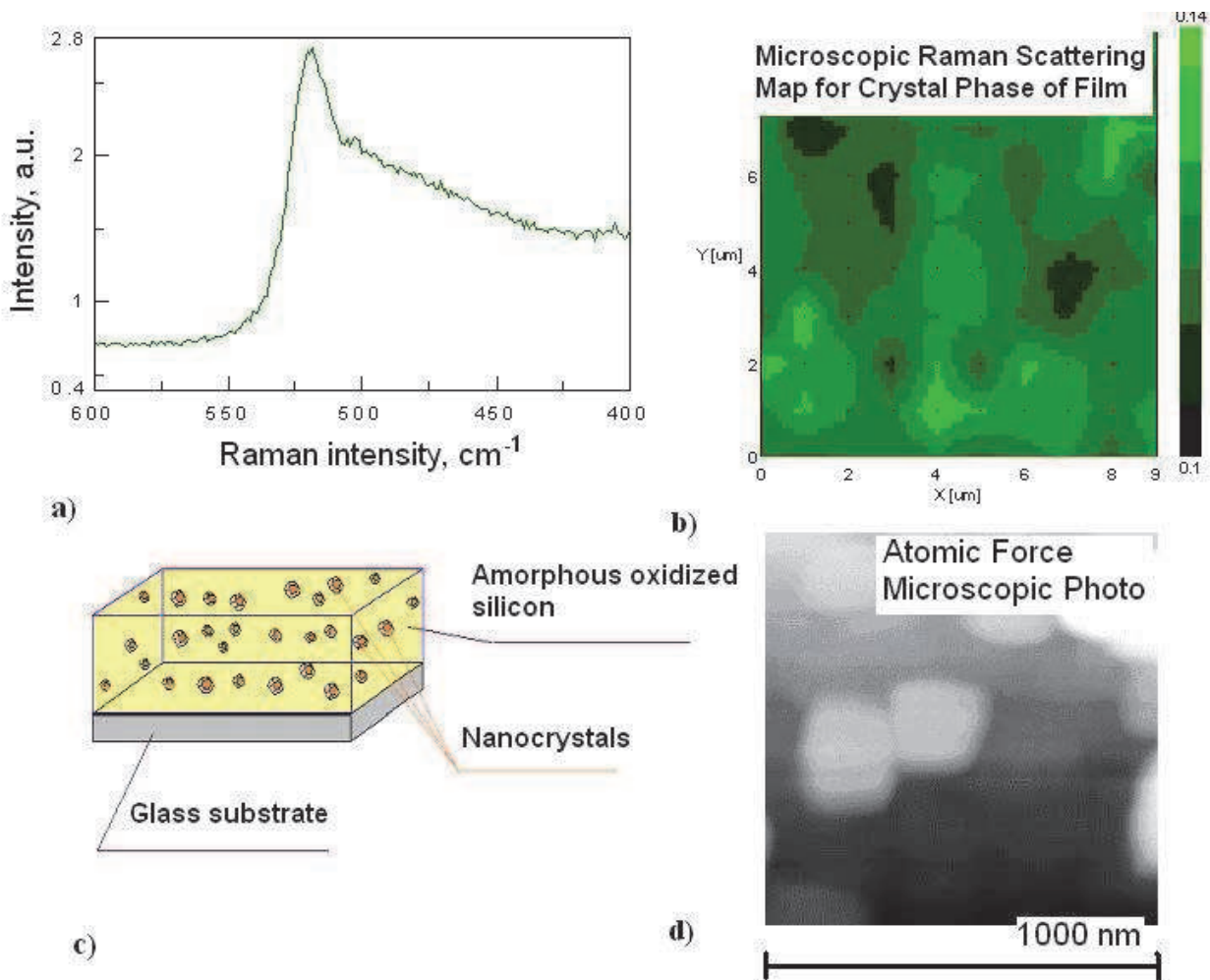


Fig. 4. Silicon nanocrystals included into silicon oxide material and their photo by means of AFM.

the presence of complex SiO configuration. Figure 5 shows the energy diagram for silicon films with nanocrystals' defects' levels, and time resolved spectroscopic data for reflected laser radiation with wavelength 532 nm for three nanocrystalline films and oxidized silicon crystal (111) surface. The wave function of excited state is a quantum interferential picture of two closed located energetic levels;

$$|\psi\rangle = a_1|\phi_1(0)\rangle \exp\left(-\left(iE_{1g}t\right) / \hbar - \Delta\omega_1t\right) + a_2|\phi_2(0)\rangle \exp\left(-\left(iE_{2g}t\right) / \hbar - \Delta\omega_2t\right); \quad (7)$$

where $|a_1|^2$ and $|a_2|^2$ are proportional to probabilities for both excited states 1 and 2. Such quantum interference of states results in quantum beats.

The Raman response (relative value in percents of all spectral area) from crystal phase of silicon around 520 cm^{-1} becomes down to three times lower by applied electric field. Width of level is $\Delta\omega=7.2 \mu\text{eV}$ and the gap between levels is $\Delta=12 \mu\text{eV}$ for silicon film with $\langle\delta\rangle=9.7 \text{ nm}$ were measured experimentally from the data of laser picosecond spectroscopy (see Fig. 5). The oxygen atoms and dimers are incorporated in the silicon grain boundary and have weak covalent bonds with silicon. But the activation energy for molecular diffusion is low, 0.3 eV, in contrast with the activation energy value for atomic diffusion (1.3 eV).

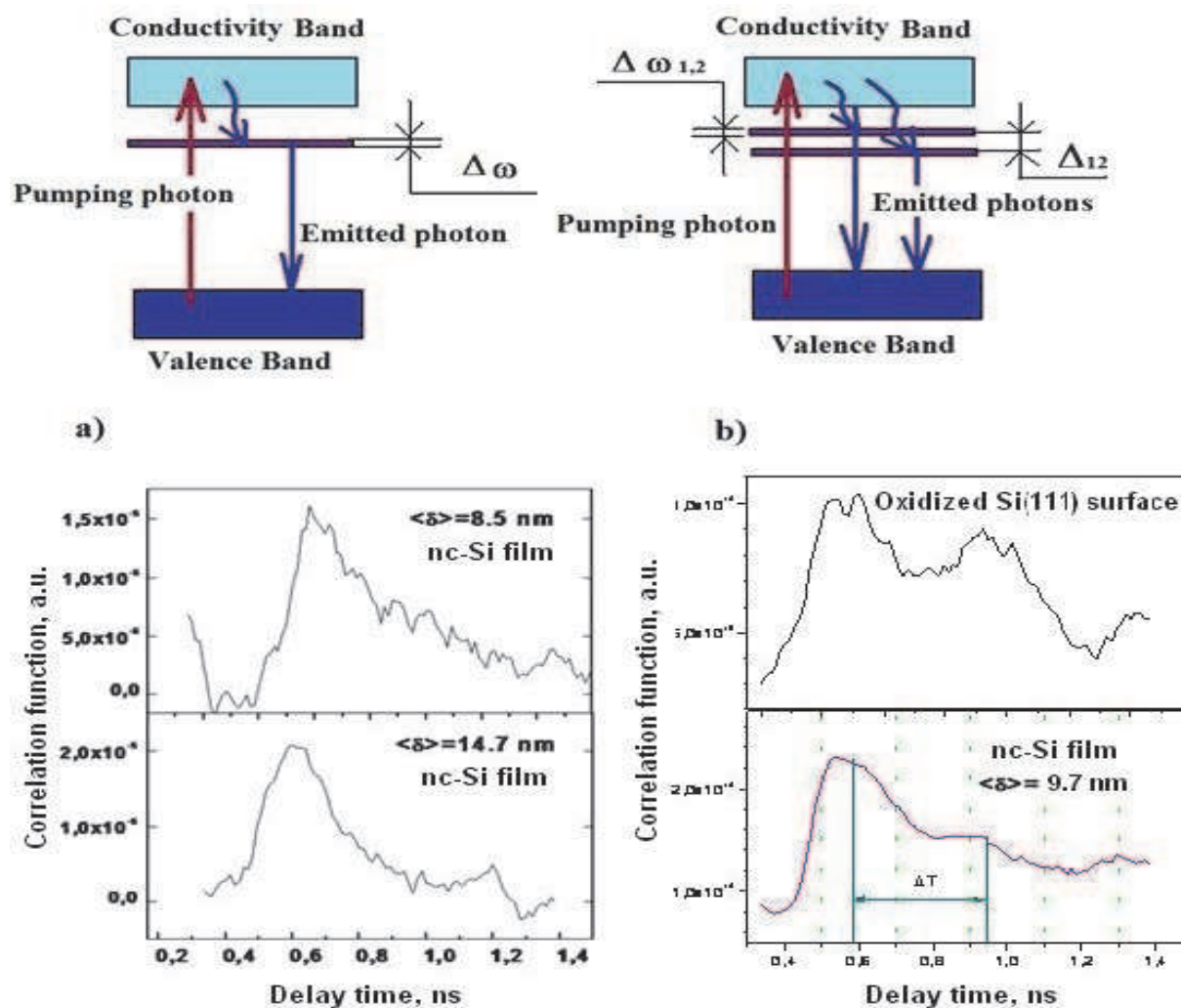


Fig. 5. Energy diagrams for different defect levels inside band gap of silicon: a) one defect level (upper graph); b) two levels which are closed to each other (upper graph); a) time evolution of excited carriers from silicon film by appearance of one defect level (down graph) near the bottom of conduction band (CB); b) quantum beats (down graph) of intensity of radiation by quantum interference of two defect levels which are closed to each other which are placed near the bottom of CB (Milovzorov, 2001).

2.5 Field effect in Raman spectra and acoustoelectric switching the optical mode

By applied electrical field the dipole moment value for Si-O-Si bridge is defined by displacement evolution:

$$\mu = \mu^0 + \mu_x(t); \quad (8)$$

The induced polarization of nanocrystalline silicon film can be explained by using the Raman scattering measurements by applied external electric field (see Fig.7). Dipole moment can be written in form (Kahan, 2000)

$$d = \frac{er}{2} \frac{(E_2 - E_1)^2}{(E_2 - E_1)^2 + 4J^2(r)} [n_2(t) - n_1(t)]; \quad (9)$$

where $n_2(t)$ and $n_1(t)$ are levels' populations, J is resonance integral, E_1 and E_2 are energies of electrons. Reflected intensity harmonic oscillations can be explained by using time dependent dipole moment of coupled atoms of Si-Si bonding. The Fermi Golden Rule for Raman scattering can be written according to (Yu & Cardona, 1996):

$$\Gamma_{Raman} = \frac{2\pi}{\hbar} \sum_{k,k'} \left| \sum_i \frac{\langle f | H_{el-phonon} | i \rangle \langle i | H_{el-photon} | 0 \rangle}{E_{i0} - \hbar\omega} \right|^2 \delta(E_c(k) - E_v(k) - \hbar\omega \pm E_p); \quad (10)$$

where $H_{electron-phonon}$ and $H_{electron-photon}$ are Hamiltonians terms for electron-phonon and electron-photon interactions.

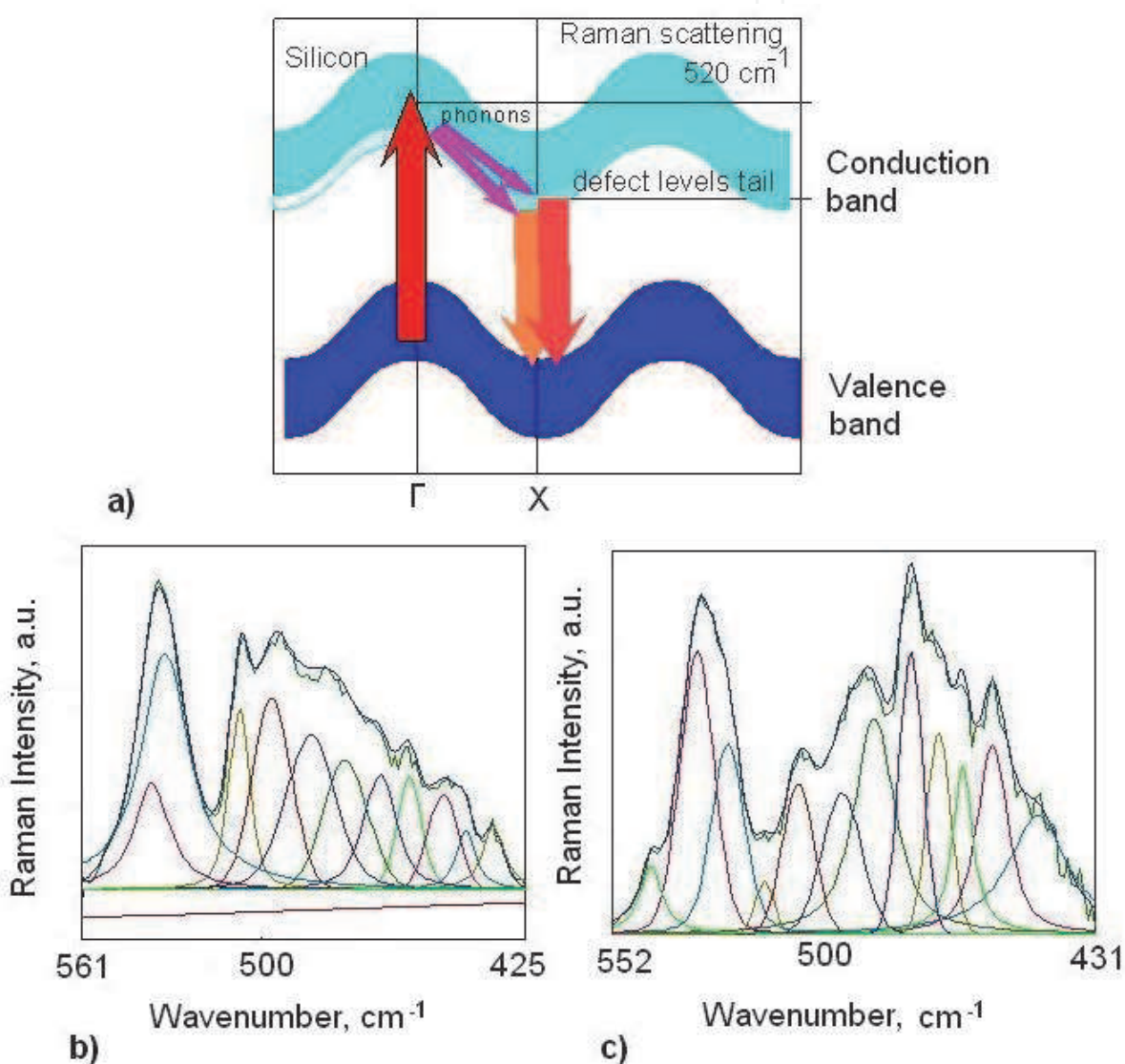


Fig. 7. Model of switching of carriers' population for silicon nanocrystals by applied electric field can be explained by using the energetic diagram of silicon film (a) and Raman scattering spectra (blue arrows) for radiation ($h\nu_{pump} - h\nu_{phonon} = h\nu_{emitted}$) with wavelength 488 nm (red arrow)) for silicon nanocrystalline films without (b) and with (c) applied electric field ($E=30 \mu V/nm$).

2.6 Field effect in Raman spectra for silicon films deposited on buffer layer

For the samples of silicon films deposited on buffer layer of cerium dioxide that was deposited at high temperature by magnetron sputtering of target the thickness of buffer layer was 90 nm. This layer was often used by thin silicon crystallized film preparation to stabilize the crystal silicon-amorphous glass disorder. This is because the crystal dielectric cerium dioxide with energy band gap 5.5 eV has the same crystal lattice constant: 5.41 Å is for CeO₂ and 5.43 Å for Si. It is seen in Figs. 8, 9 the Raman spectral data for various external applied electrical field values from silicon film deposited on buffer cerium dioxide layer at low deposition temperature with crystal fraction less than 30%. Figure 8 illustrates the changes in phonon modes which were occur by applying the external electric field. It is seen, that the crystal-related spectral peak is decomposed into two component (LO and TO phonon modes) with their energy positions at 515 cm⁻¹ and 524 cm⁻¹ without field (E=0), and 514 cm⁻¹ and 524 cm⁻¹ by E≠0. Figure 9 illustrates the lowering in the magnitude of LO phonon modes by increasing the external electric field. In this case the dipoles in polarized buffer layer generate the electric field which is sufficient for stabilizing the nanocrystals inside the silicon film. Because, there is phonon TO-LO modes splitting which is observed in Fig.8.

2.7 Raman silicon laser development

According to the work of (Klein & Cook, 1967) the solution of transformed Maxwell's equations can be written as combination of plane waves. For the plane wave (with frequency ω) incident on the film and interacted with phonons wavelength Λ the intensity of radiation is represented by ($\Lambda \leq 0.01\omega$):

$$I = I_0 W^2 \frac{\sin\left(\frac{X\pi L}{\Lambda \cos\theta}\right)}{X}; \text{ where } X^2 = W^2 + (\sin\theta_B - \sin\theta)^2; W = \frac{\Lambda}{2\lambda} \frac{\Delta\varepsilon}{\varepsilon}. I_0 \text{ is intensity of the}$$

incident laser radiation, $\Delta\varepsilon$ is a perturbation of dielectric function by phonons or electric fields. The spectral width of output radiation depends on the geometrical ratio between thickness of film d (see Fig. 10) and substrate ℓ , and wavelength of radiation. By applying the external electric field the dielectric function is varied and the spectral width is, also, changed. The cavity with length d is adjusted according to following requirements:

$$\Delta\nu = \frac{c}{2nd}; d = m\lambda.$$

The quality factor of cavity Q characterizes the degree of spectral sharpness of output radiation (Verdeyen, 1995):

$$Q = \frac{2\pi nd}{\lambda_0} \frac{(r_1 r_2)^{1/4}}{1 - (r_1 r_2)^{1/2}}. \quad (11)$$

The edge reflectivities r_1, r_2 are sufficient (~ 0.5), and their values depend on Si/SiO₂ interface. By the addition the CeO₂ buffer layer with strong polarization property with thickness more than 50 nm the efficient transfusion of laser energy into TM or TE mode by applying the external field can be easily achieved. It is reflected in spectral pictures that there is a splitting of TO and LO phonon modes by assisted electric field.

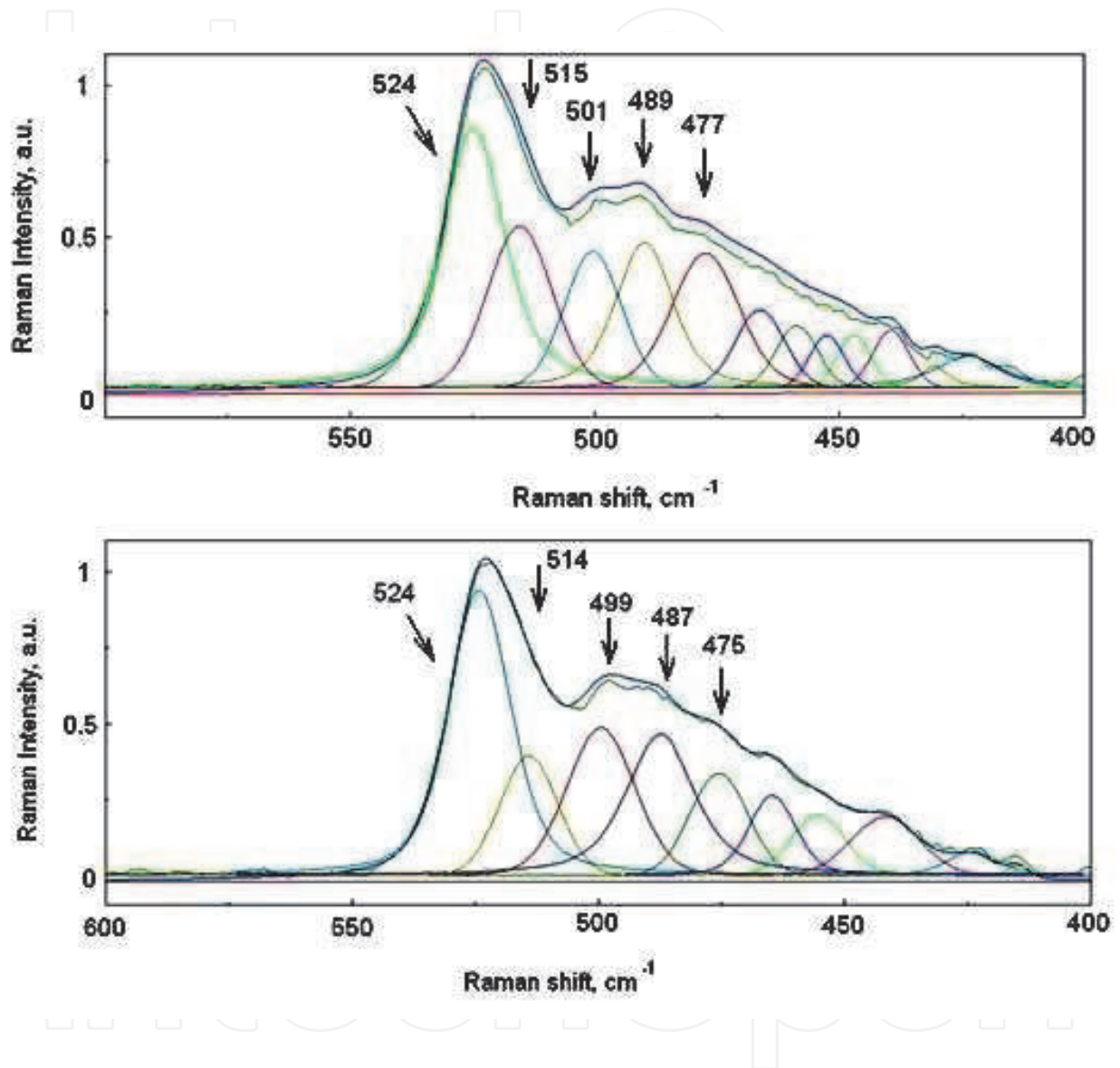


Fig. 8. Raman spectra from silicon film deposited on buffer layer without (upper graph) and by applied external electric field (down graph).

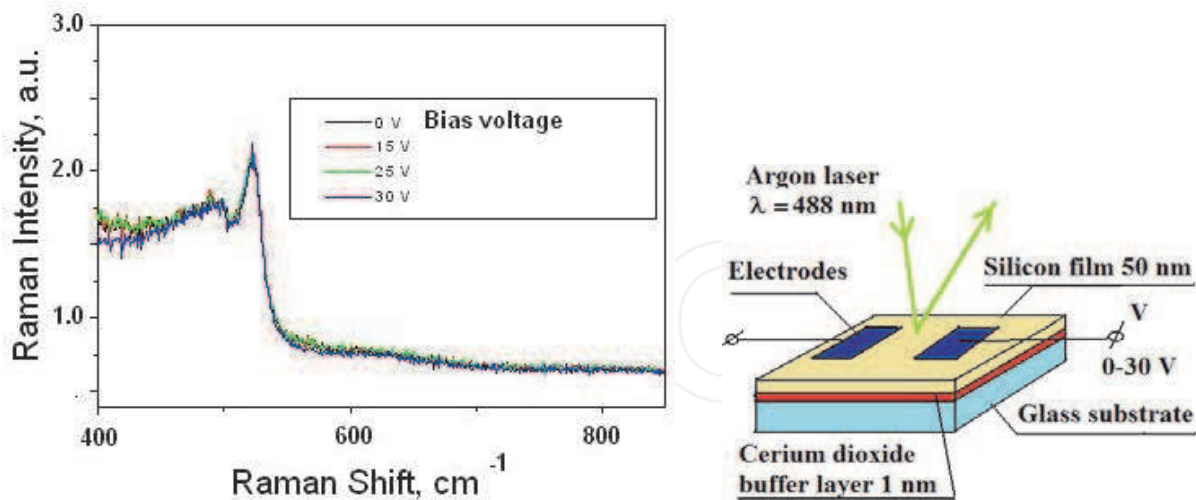


Fig. 9. Raman spectra (left graph) from nanocrystalline silicon film deposited at low temperature on buffer layer of cerium dioxide with thickness 90 nm: a) 0V/cm; b) 30V/cm; c) 50V/cm; d) 60 V/cm. Scheme of acoustoelectric switcher for laser optical modes (right graph).

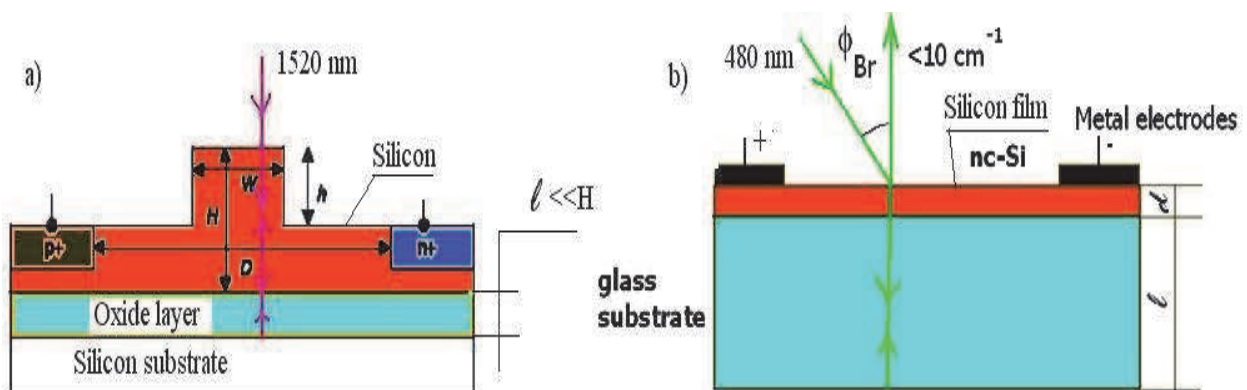


Fig. 10. Typical scheme of ordinary Raman silicon laser (a) and laser cavity for Raman scattered radiation with two separate TM and TE modes (b) based on thin film and glass substrate.

3. Nonlinear optical switchers and lasers

3.1 Chemical bonds as quantum objects

3.1.1 FT-IR spectral components and SHG response

Figure 11 shows the SHG spectra from two silicon films (prepared by using PECVD and gas mixture of silane and hydrogen) with nanocrystals Gauss distributed in their sizes and crystalline volume fraction 60%. There is a slight difference in standard deviation of Gauss distributions functions for nanocrystals' sizes in the area of 1 mm² (laser beam diameter on the film). It is clear, that by the same physical properties, chemical contamination, and structural properties the SHG signals is significant varied. This is because of dipole appearance inside silicon film. There is great variations in chemical bonding of silicon and oxygen (or hydrogen and fluorine), kinds of point defects and their spatial distribution which contribute in local field factor. The bond length distortion causes the surface strain. This is because of there is an oxygen atoms incorporation and structural relaxation of

surface Si atoms (see Figs.12, 13 a, b). ShklyaeV and coworkers (ShklyaeV et al., 1999) proposed the model of oxygen nucleation on the silicon surface. There are several critical conditions in oxygen interaction with silicon. The kinetic of Si surface oxidation was studied by SHG method. However, there are no evident information about earlier lateral growth and oxygen adatoms. Figure 12 illustrates the spectral peaks around 1100 cm^{-1} (upper graph) corresponded to the oxygen triplet states ($^3P_{2-0}$) in poly-Si films FTIR spectra. It is supposed that oxygen molecules are inserted in interface amorphous media between silicon nanocrystals and cause the appearance of three spectral peaks around 1100 cm^{-1} . It is assumed that the contents of crystallite structure Si-O-O-Si is low, but the Si-O-O-O-S is sufficient. There are no triplet states related spectral peaks for buried silicon oxide, by the annealing to the temperature 1100°C . The quartz Si-O-Si bridging structure produces one peak at 1100 cm^{-1} with great magnitude. The spectral splitting of 0.008 eV is because there are two unpaired electrons at two p orbital. However, the lateral position is unpredictable due to the great value of the surface diffusion. It is assumed, that the defects are localized in Si-SiO₂ interface with complex composition SiO_x. The increase in oxygen concentration per silicon atom x results in increasing of SiO bond length. For the sample with smaller grain size the hydrogen termination of dangling bonds is greater, and density of oxygen is low. But, the film with large grains contains great amount of oxygen in Si-O-Si and SiO₂ compositions. Also, it is assumed that the exponential electron density decay is due to the exciton state decay. The short relaxation time can be described as possible relaxation process through the oxygen incorporation related defect states, which density of states is following: $n(E)=(n_{\text{Si}}(E)+xn_o(E))/(1+x)$ [22] (Lanoo & Allan, 1978; Delerue et al., 1993). For low graph in Fig.12 the silicon film has crystalline volume fraction 48%, and nonlinear responses in various ranges of SHG spectra are following: $I_{\text{shg}}=1.65$ at $\lambda_{2\omega}=370\text{ nm}$; $I_{\text{shg}}=0.9$ at $\lambda_{2\omega}=535\text{ nm}$; $I_{\text{shg}}=0.5$ at $\lambda_{2\omega}=420\text{ nm}$.

3.1.2 Nonlinear optical signal by chemical bonding variations

The radiation with determined wavelengths for second-harmonic generation was detected for a films deposited on glass, silicon (100) and quartz substrates. The film thickness was more than 300 nm. Figure 13 shows the absorbances of different silicon films prepared by using gas mixture of silane diluted by hydrogen and silicon tetrafluoride diluted by helium as 5:95. It is seen, that there is great variations in chemical bonding properties of films. It is supposed that the spectral lines at 1107 cm^{-1} (see Fig. 13 b) is related to the asymmetric stretching mode for Si-O-Si of interstitial oxygen atom; the spectral line at 913 cm^{-1} (see Fig. 13 c) is for SiH₃ bending mode; the spectral peak at 1174 cm^{-1} (see Fig.13 b) is an asymmetric stretching mode of O-Si-O TO (Wang et al. , 1999), and line at 1060 cm^{-1} (see Fig. 13 b) is for stretching mode of O-Si-O bonding (TO mode in phase motion of oxygen atoms) (Wang et al., 1999); spectral line at 956 cm^{-1} (see Fig. 13 d) as scissor mode of Si-H₂ (Chabal et al., 2002), spectral lines at 975 cm^{-1} and 979 cm^{-1} (see Figs. 13c, 13d) are related to silicon fluorine bonding (Milovzorov et al., 1998, Milovzorov, 2010) or divalent silicon specy interacted with two oxygen atoms (Chabal et al., 2002); spectral lines at 902 cm^{-1} (see Fig. 13c) and 901 cm^{-1} (see Fig.13d) are related to silicon hydrogen bonding Si-H₂ scissor mode (Chabal et al., 2002); also, spectral line at 913 cm^{-1} corresponds to the Si-F₅ molecular-like assembly (King et al., 1986); and spectral line at 934 cm^{-1} (see Fig. 13b) and 933 cm^{-1} (see Fig. 13d) are related to stretching mode Si-F of Si₉H₁₅F configuration (Chatterjee et al., 2001) ; spectral lines at 838 cm^{-1} (see Fig. 13d) and 841 cm^{-1} (see Fig.13c) are related to A-center response (Corbett et al., 1961, 1964). In addition, it is assumed that the spectral lines at 858 cm^{-1} (see Fig. 13d) and at

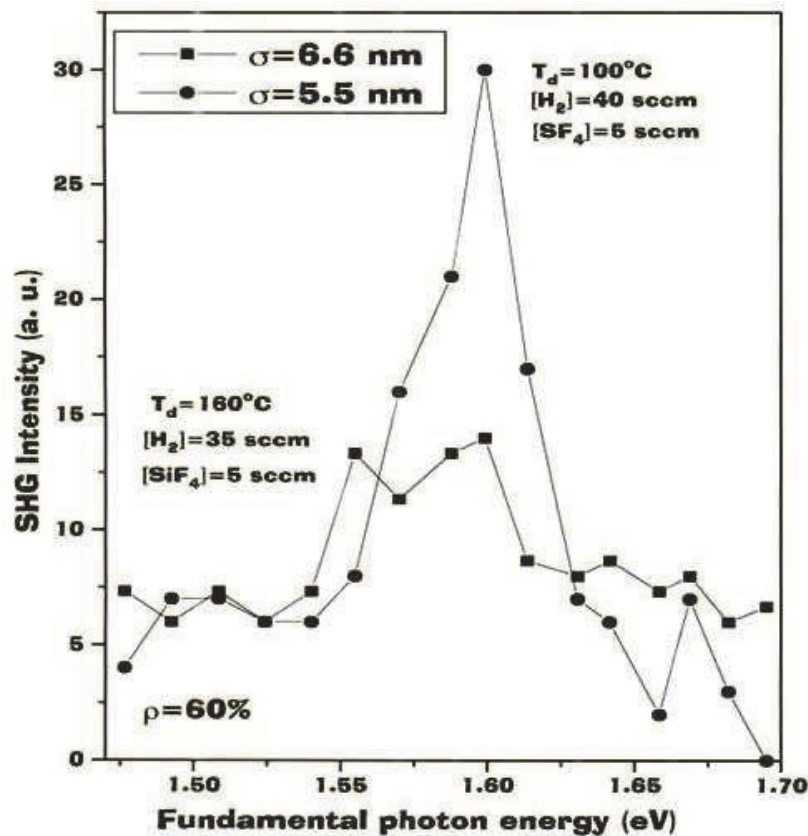


Fig. 11. SHG spectra from silicon films with nanocrystals Gauss distributed in their sizes and crystalline volume fraction 60%.

859 cm^{-1} (see Fig. 13c) is for Si-F stretching mode or Si=O stretching mode of silylene and electron configuration for the triplet state.

Variation in SHG signal for different nanocrystalline films with their chemical bonding properties at determined wavelengths is presented in Table № 1. In addition, there is SHG responses from the films with silicon substrate, crystalline volume fractions obtained by using Raman data, average grain sizes of nanocrystals estimated by means of X-ray diffraction, and photoluminescent signal. It is supposed that the SHG spectrum is produced by surface component of dipole moment because there is a violence of symmetry by surface and great contribution into the surface area of large size nanocrystals (S/V ratio). The great enhance is due to the appearance of surface's nonzero dipole moment:

$$P^S(2\omega) = \chi_{\text{surface}}^{(2)} : E(\omega)E(\omega) + \chi_{\text{Si-O:F}}^{(2)} : E(\omega)E(\omega) + \chi_{\text{distortion}}^{(2)} : E(\omega)E(\omega). \quad (12)$$

There is anisotropy of nonlinear optical properties by the dominant crystal orientation (111) for the films deposited at low temperatures. Such kind of anisotropy can be easily recognized by means of p- or s-polarized laser radiation and by the detection of s-polarized, for χ_{xxx} or χ_{zzz} components or p-polarized, for χ_{zzz} , χ_{zxx} and χ_{xxz} components of output radiation. The nonlinear second-order susceptibility depends on the surface hydrogen coverage θ_H according to the formula (Durr & Hofer, 2006):

$$\chi_{s,j,k}^{(2)}(\theta) = \chi_{zzz} + (1 - \theta_H)\chi_{xxz} \quad (13)$$

where χ_{zzz} and χ_{xxz} are the nonzero tensor components of susceptibility, $0 \leq \theta_H \leq 1$ ML.

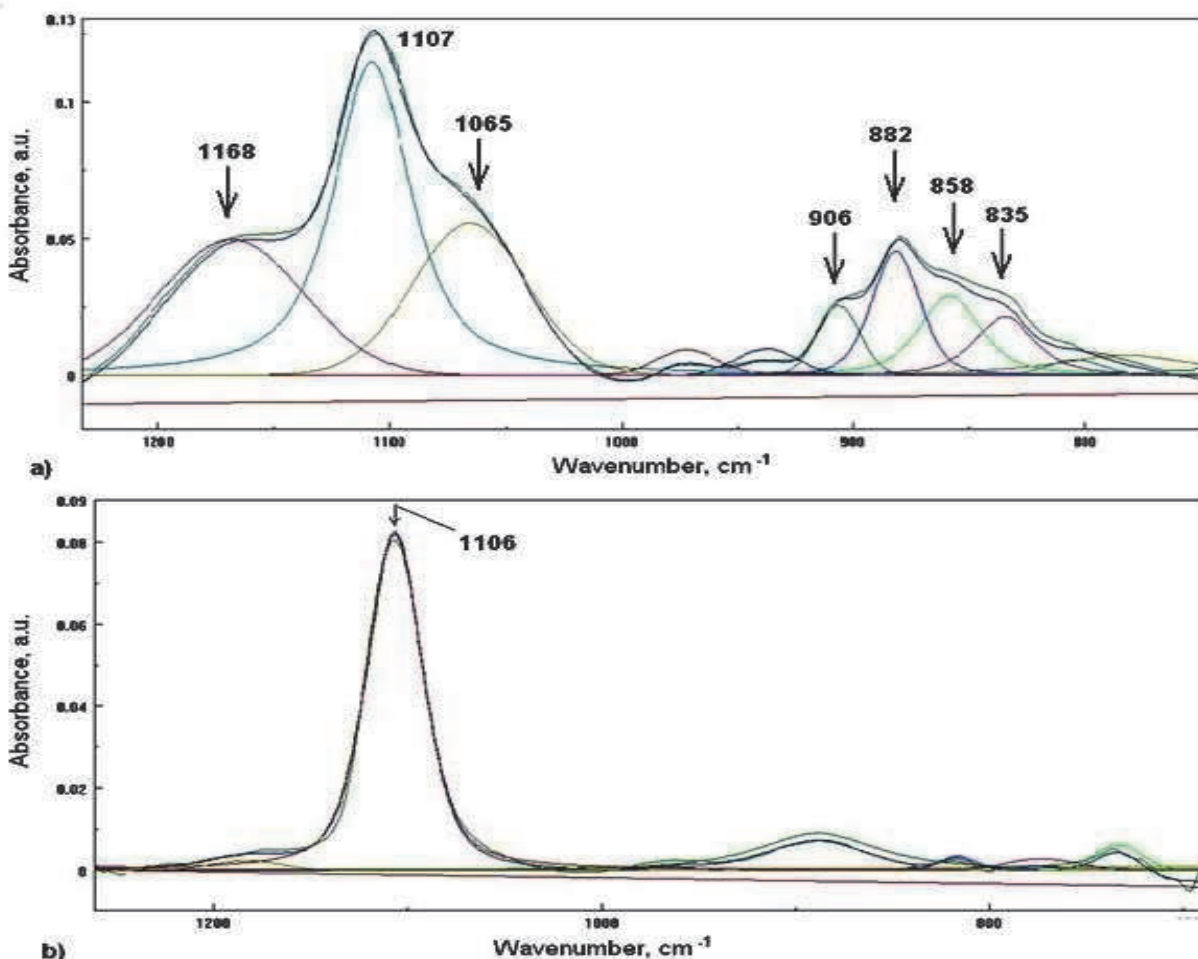


Fig. 12. FT-IR spectra from oxidized nanocrystalline silicon films (a) and (b) with significant SHG response.

3.2 Dipole moments and SHG spectra

The nature of defects is complicated because the types of oxygen (or fluorine) and hydrogen incorporation in nc-Si films are varied. There are different kinds of defects with significant physical properties such as paramagnetic centers or charge traps. The optical luminescent properties depend on defect density and their spatial distribution. Optical absorption measurements help to study the oxygen and hydrogen incorporation, to characterize the types of defects, to evaluate the density of bonds. Dipole moment of silicon dangling bond can be estimated by using combination of $Si(1s)-Si_{db}(3p)$ and $Si(3p)-Si_{db}(3p)$ atomic orbital:

$$\begin{aligned} \mu &= ed \int_0^{V_{2\xi}} \Psi_{Si1s} \Psi_{Si3p} dv; \\ \mu &= ed \int_0^{V_{2\xi}} \Psi_{Si3p} \Psi_{Si3p} dv; \end{aligned} \tag{14}$$

where the value $V_{2\xi}$ is the volume of integration. The overlap integrals are shown in the Table № 2 to calculate the dipole moment values.

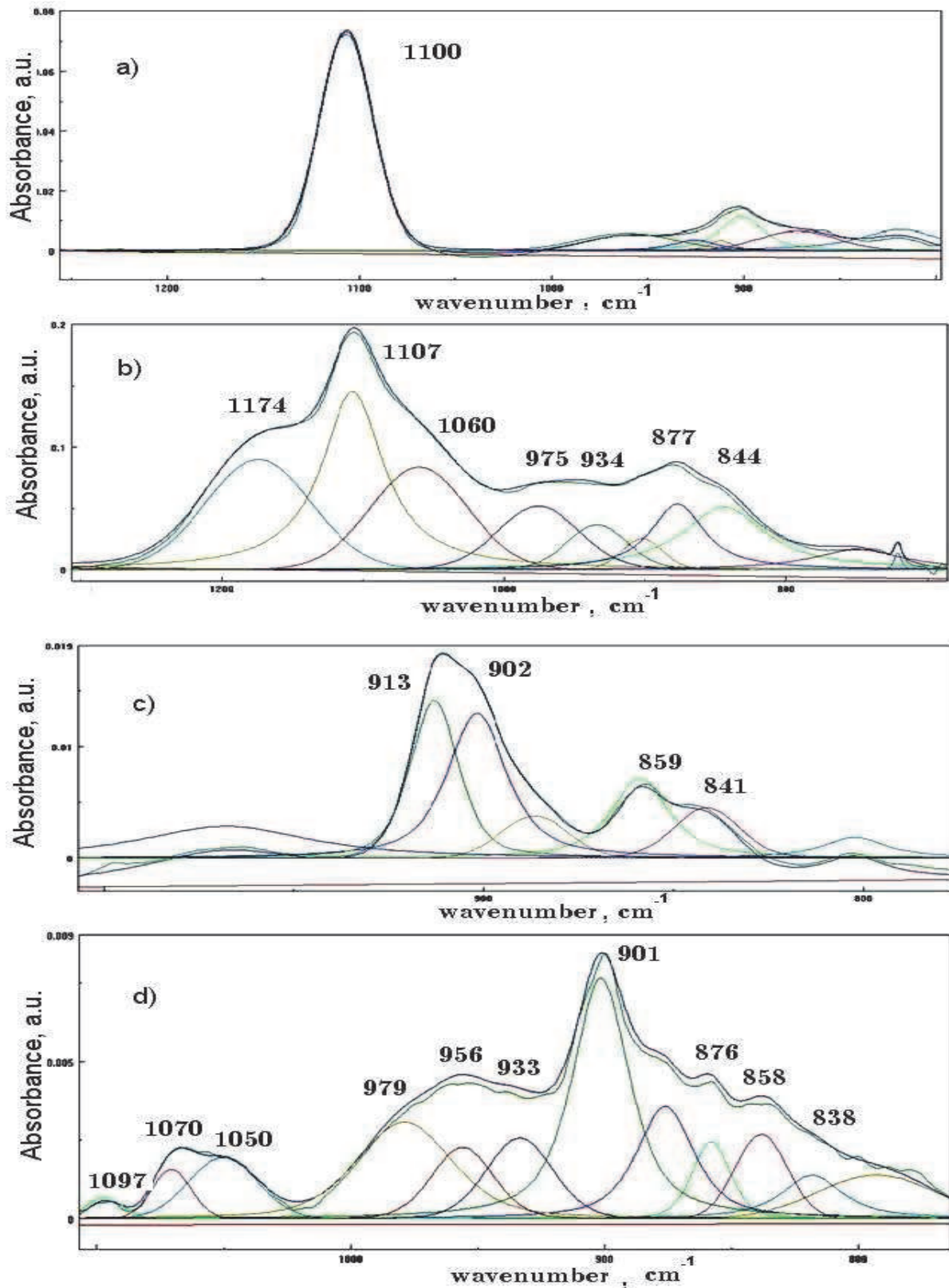


Fig. 13. FT-IR spectra for nanocrystalline silicon films with high SHG response in UV and visible range; silicon films are varied in chemical bondings: a) SD56, b) SD 55, c) SD 58, d) SD53. The SHG signals for all films are in Table № 1.

Sample, Chemical bonding	$\lambda=370$ nm	$\lambda=420$ nm	$\lambda=450$ nm	$\lambda=472$ nm	$\lambda=535$ nm	Silicon substrate $\lambda=420$ nm	Silicon substrate $\lambda=450$ nm	Silicon substrate $\lambda=535$ nm	nc-Si Size, nm	$\rho, \%$	PL
SD52, Si-O-Si bridge	1.13	0.052	1.06	0.7	17	1.5	1.2	17	10	70	PL
SD53, Si-F	1.06	10	1.5	0.7	10	0.7	2.0	20	11	70	PL
SD55, Si-O	1.65	0.02	0.73	0.3	13	0.12	0.6	20	-	30	PL
SD56, Si-O-Si	0.75	0.04	2.0	0.7	10	1.0	24	-	18	70	PL
SD58, Si-F	0.47	0.9	1.8	0.7	10	0.2	1.0	15	-	30	PL

Table 1. SHG signals detected on fixed wavelengths from the 5 different silicon films with various fractions of nanocrystals, deposited on glass and silicon (100) substrates.

d , length for strain or broken bond, Å	Overlap integral value for silicon $3p$ - $3p$ orbital, δ_2 10^{-6}	Overlap integral value for silicon $3p$ - oxygen $2p$ orbital, δ_3 10^{-6}
3.65	$6.835 \cdot 10^4$	$3.1 \cdot 10^{-4}$
2.21	$8.37 \cdot 10^5$	2.8
2.35	$6.75 \cdot 10^5$	1.2
3.83	$4.84 \cdot 10^4$	$9.55 \cdot 10^{-5}$

Table 2. The overlap integral values calculated for silicon bonds and silicon-oxygen bonding at fixed bond lengths.

For the silicon orbital ($1s$)-oxygen atom orbital ($2p$) and silicon orbital ($3p$)-oxygen orbital ($2p$) interactions we can evaluate dipole moment of Si-O bond by using formula:

$$\begin{aligned} \mu_{2pO-3pSi} &= ed \int_0^{2\xi} \Psi_{O2p} \Psi_{Si3p} dv; \\ \mu_{2pO-1sSi} &= ed \int_0^{2\xi} \Psi_{O2p} \Psi_{Si1s} dv \end{aligned} \tag{15}$$

where d is bond length, $dv = 4\pi r^2 dr d\phi d\theta$, $0 < r \leq 2\xi$, ξ is a largest covalent radius. By the $r = 1.6 \text{ \AA}$, $r/a_0 = 3$ the value $\mu_{2pO-3pSi} = 1.12D$.

Figure 14 illustrates the nonlinear spectra because the SHG response is optically induced in oxidized nanocrystalline silicon films. There are various phenomena which can be responsible for increasing the SHG. The first possible explanation of nonlinear optical properties is appearance of dipoles inside the film such as Si-O bonding with significant dipole moment. The second is a perturbation of electron density by electromagnetic field by

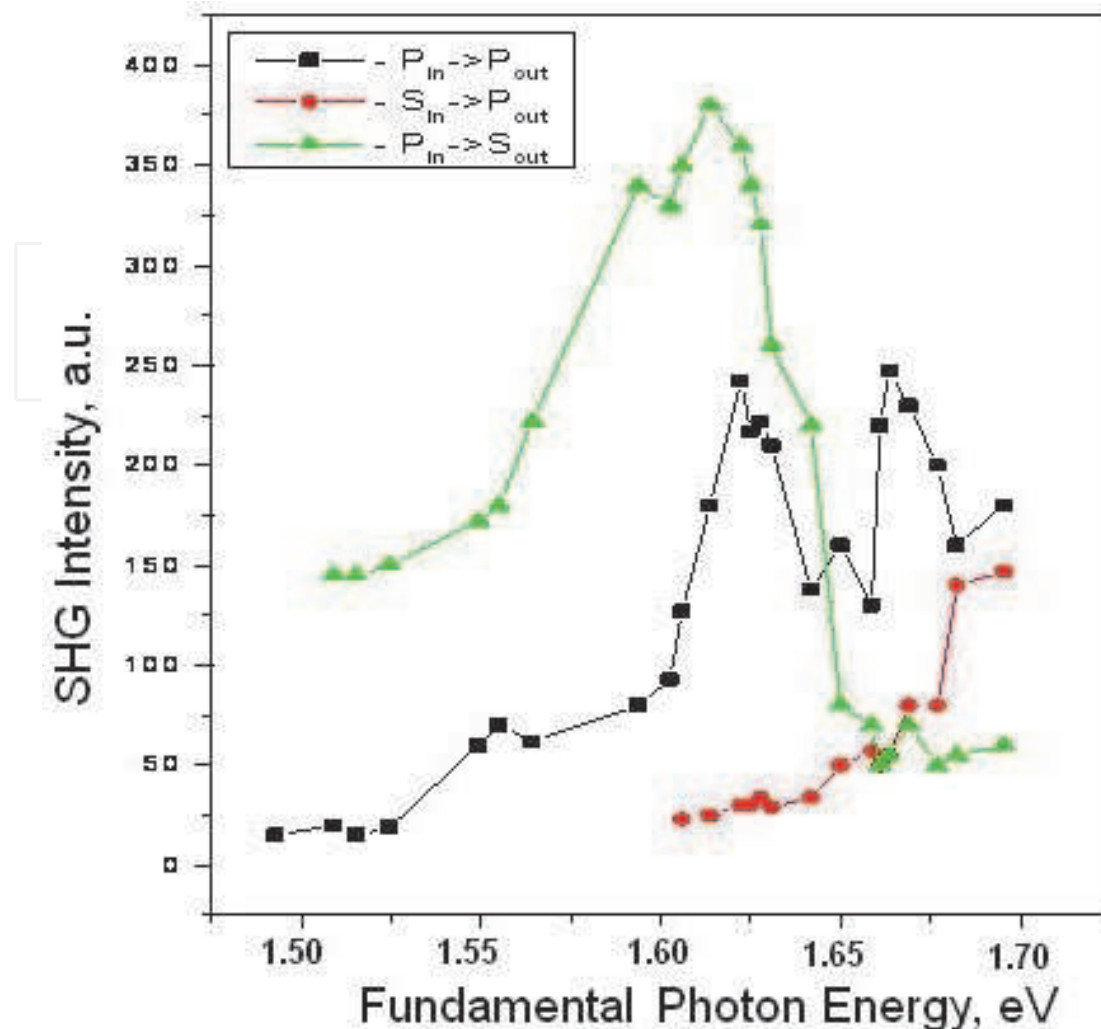


Fig. 14. Nonlinear SHG spectra from the surface of silicon films with 10 nm-sized nanocrystals (111) and crystalline volume fraction at 70%.

applied external electric field or laser field. The third is a quadruple moments from the complex point defects, such as vacancy of oxygen atoms in Si/SiO₂ interface area, dangling bonds which migrate in films due to the weakening of silicon bonds. It is supposed, the value of dipole moment by the angle between the two Si-O bonds is around 109°. The second-order terms of dipole values for polarized media are given by

$$\mu^{(2)} = e \int_0^{V_R} \Psi_{Si1s} \Psi_{Si3p} dv \left(\int_0^{V_R} \Psi_{Si1s} x^2 \Psi_{Si3p} dv - \left(\int_0^{V_R} \Psi_{Si1s} x \Psi_{Si3p} dv \right)^2 \right) / \int_0^{V_R} \Psi_{Si1s} x \Psi_{Si3p} dv \quad (16)$$

where a sphere of integration is V_R , x is bond length. It is assumed that x value is a sum of two covalent radii for both atoms, ξ is a largest covalent radius for two atoms, R is a distance by the atomic orbital for each center has spatial the limit of its extension, for the values of distance $R = 4\xi$ we suppose the averaging procedure is possible. This dipole moment is because of the dangling bond causes the breaking in crystal structure's symmetry. The concentration of dangling bonds in silicon film deposited on glass substrate is varied from 10^{16} cm^{-3} to 10^{20} cm^{-3} .

The next two types of dipole moments are due to the oxygen atom incorporation with silicon can be evaluated for determination the role of oxidized silicon in yield of second-harmonic generation:

$$\begin{aligned} \mu^{(2)} &= e \int_0^{vR} \Psi_{Si1S} \Psi_{O2p} dv \left(\int_0^{vR} \Psi_{Si1S} x^2 \Psi_{O2p} dv - \left(\int_0^{vR} \Psi_{Si1S} x \Psi_{O2p} dv \right)^2 \right) / \int_0^{vR} \Psi_{Si1S} x \Psi_{O2p} dv; \\ \mu^{(2)} &= e \int_0^{vR} \Psi_{Si3p} \Psi_{O2p} dv \left(\int_0^{vR} \Psi_{Si3p} x^2 \Psi_{O2p} dv - \left(\int_0^{vR} \Psi_{Si3p} x \Psi_{O2p} dv \right)^2 \right) / \int_0^{vR} \Psi_{Si3p} x \Psi_{O2p} dv; \end{aligned} \tag{17}$$

The first integral in equation describes the charge spatial distribution of two atomic orbital that are located on different centers overlap. The second term in such multiplication in brackets describes the spatial distortion of dipole bond length by various conditions: such as external electromagnetic field or the other coupled $Si - O$ dipole. These changes cause the perturbations in wave functions, too. However, we estimate such dipole moment distortion by using non perturbative wave functions and stressed bond with its length more than ordinary. Such dipole moment deviation causes the electron density distortion and significant nonlinear optical signal. In addition, the induced by external field dipole moment for a pair of silicon atoms can be explained as following:

$$\begin{aligned} \mu_{\bar{Si}-Si}(t) &= ed \left(\int_0^{v2\xi} \Psi_{3p\bar{Si}}(t) \Psi^*(t)_{3pSi} dv + \int_0^{v2\xi} \Psi_{1s\bar{Si}}(t) \Psi^*(t)_{1sSi} dv + \int_0^{v2\xi} \Psi_{3p\bar{Si}}(t) \Psi^*(t)_{1sSi} dv + \int_0^{v2\xi} \Psi_{1s\bar{Si}}(t) \Psi^*(t)_{3pSi} dv \right); \\ \Psi_{3p\bar{Si}} &= \Psi_{3pI} \exp(-iE_{3pI}t / \hbar) + \Psi_{3pII} \exp(-iE_{3pII}t / \hbar); \\ \Psi_{1s\bar{Si}} &= \Psi_{1sI} \exp(-iE_{1sI}t / \hbar) + \Psi_{1sII} \exp(-iE_{1sII}t / \hbar). \end{aligned} \tag{18}$$

The wavefunctions according to the P. Feuer theoretical work (Feuer, 1952) corresponding to the energies E_I and E_{II} by external applied electromagnetic field can be written as

$$\begin{aligned} \Psi_I &= \frac{1}{\sqrt{2}} \sum_m (J_{m+1}(-q_1) a_1(x - x_m) + (J_{m+2}(-q_2) a_2(x - x_m)); \\ \Psi_{II} &= \frac{1}{\sqrt{2}} \sum_m (J_{m+1}(-q_1) a_1(x - x_m) - (J_{m+2}(-q_2) a_2(x - x_m)). \end{aligned}$$

Here, the J_m is a Bessel function and Taylor expansion of perturbing potential is $V(x) = eFx_m + eF(x - x_m)$.

3.3 χ^2 susceptibility components from polarized light experiments

For spectral measurements, an optical parametric oscillator/amplifier pumped by the third harmonics (0.355 nm) of a Q-switched Nd:YAG laser (Spectra-Physics, MOPO 730) at a 10 Hz repetition rate was used. The p-polarized laser radiation with spectral width of 0.3 cm^{-1} was focused on the sample to a spot with diameter of 0.5 mm. The energy of primary laser radiation was near 3 mJ. Resonance spectra consist of two sharp peaks. The peak at 1.6 eV is caused by SHG response due to $E_0' = \Gamma_{25} - \Gamma_{15}$ transition. We suppose that the second peak can be recognized as SHG response due to $E_1 = L_2 - L_1$ transition in silicon nanocrystallites.

It is observed the sharp spectral peaks around 3.26 eV related to SiO bonding in silicon network with energy position $E_c - 0.14 \text{ eV}$ (see Figs. 15-16). It is assumed, that the second

sharp peak is related to vacancy of oxygen switching by A-defects (with energy position $E_c - 0.17$ eV for bulk Si) appearance in silicon films. It can be observed by means of spectroscopic methods (such as FT-IR, EPR, Laser time-resolved spectroscopy) only in fluorinated silicon films. A-defects were detected at first time in silicon irradiated by high energy electron beam by (Watkins & Corbett, 1961). For silicon film synthesized by PECVD method there is H_2SiF_6 acid and ortho-silicon acid which generate nonlinear response due to their great dipole moment. Such incorporation is changed according to fluorine dilution. The SiO bonding decreases, but the angle of $Si-O-Si$ bridge is changed, there is a $Si-Si$ atomic orbital splitting. The two new levels are closed to each other with difference around several μeV (see Fig. 5b). Figure 16 illustrates the SHG spectra for $P_{in} \rightarrow S_{out}$ polarization scheme for horizontal (left graph) and vertical (right graph) spatial positions of sample with nanocrystalline silicon film with average grain size 97 Å. SHG spectra contains isotropic and anisotropic component of susceptibility tensor $\chi^{(2)}_{zzz}$, $\chi^{(2)}_{zxx}$, $\chi^{(2)}_{xxz}$ and $\chi^{(2)}_{xxx}$. Figure 17 illustrates the second-harmonic generation by optical pumping of laser light with energy of pumping photon 1.63 eV (black arrow) along with resonant tunneling of carriers through the thin layer of amorphous oxidized silicon. The pumping photons energies $h\omega$ are 1.63 eV, but the emitted second-harmonic photons with $2h\omega$ energies (3.26 eV) have the: $2h\omega_{emitted} = h\omega_{pumping} + h\omega_{pumping}$. The red arrow corresponds the pumping photons with summ energies more than 3.4 eV (for direct transitions in bulk Si (111)), and the blue arrows illustrate the photoluminescent radiation, caused by optical transitions through the excited levels which are situated inside band gap of silicon, too. It is necessary to note, that the resonant tunneling processes can be realized from the level with lower energy to the next energy level in closed silicon nanocrystal (see Fig. 17) or other defect levels inside oxidized silicon layer. It is clear, that by the resonance tunneling the population of lower levels decreases but the population of upper levels increases.

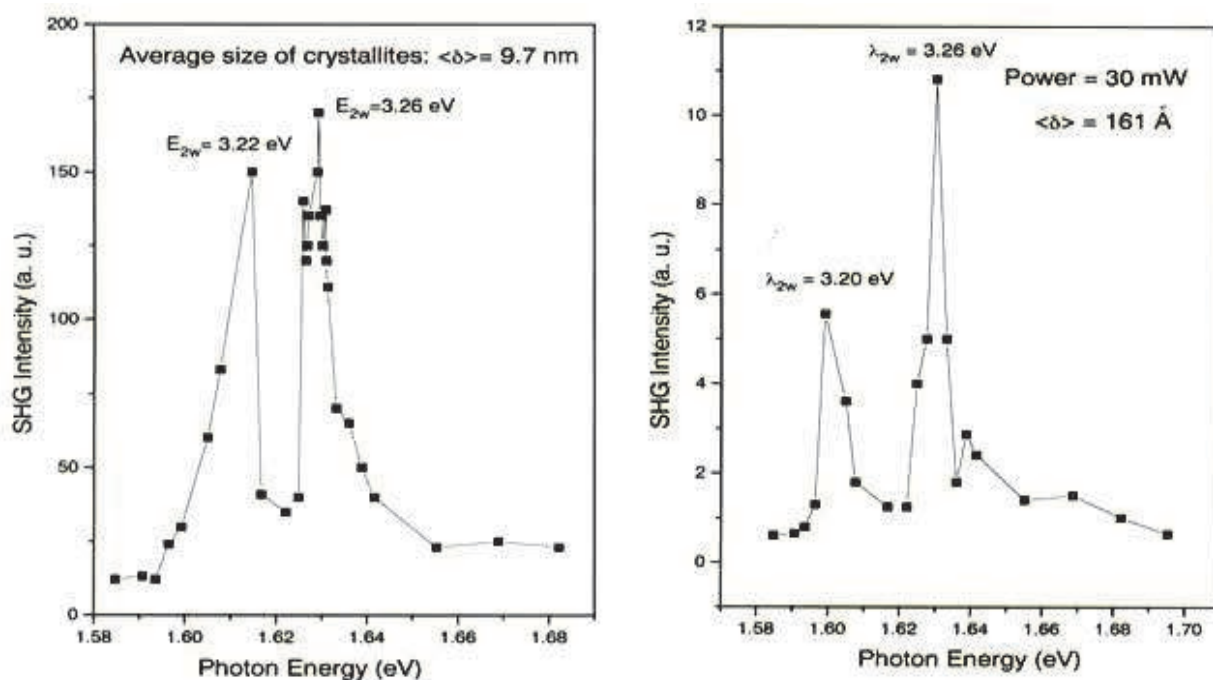


Fig. 15. SHG spectra ($P_{in} \rightarrow P_{out}$) for $\chi^{(2)}_{xxx}$ component of susceptibility tensor for nanocrystalline silicon films with average grain sizes 97 Å (left graph) and 161 Å (right graph).

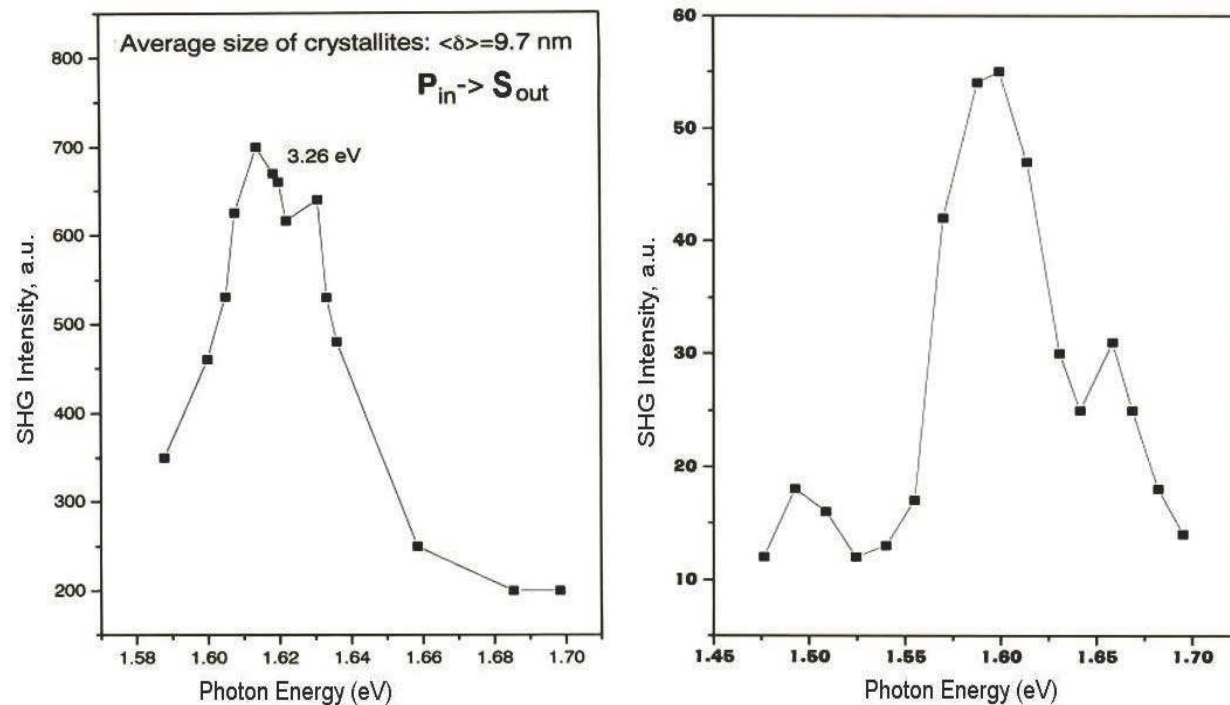


Fig. 16. SHG spectra for $P_{in} \rightarrow S_{out}$ polarization scheme for horizontal (left graph) and vertical (right graph) spatial positions of sample.

The nonresonant SHG intensity as a function of the average grain size in poly-Si films, with crystalline volume fraction 70%, is presented in Fig. 18, where

$$K = \frac{I_{exp}}{I_{exp}^{min}} \frac{|L(2\omega, \rho_{min})L^2(\omega, \rho_{min})|}{|L(2\omega, \rho)L^2(\omega, \rho)|} \quad (19)$$

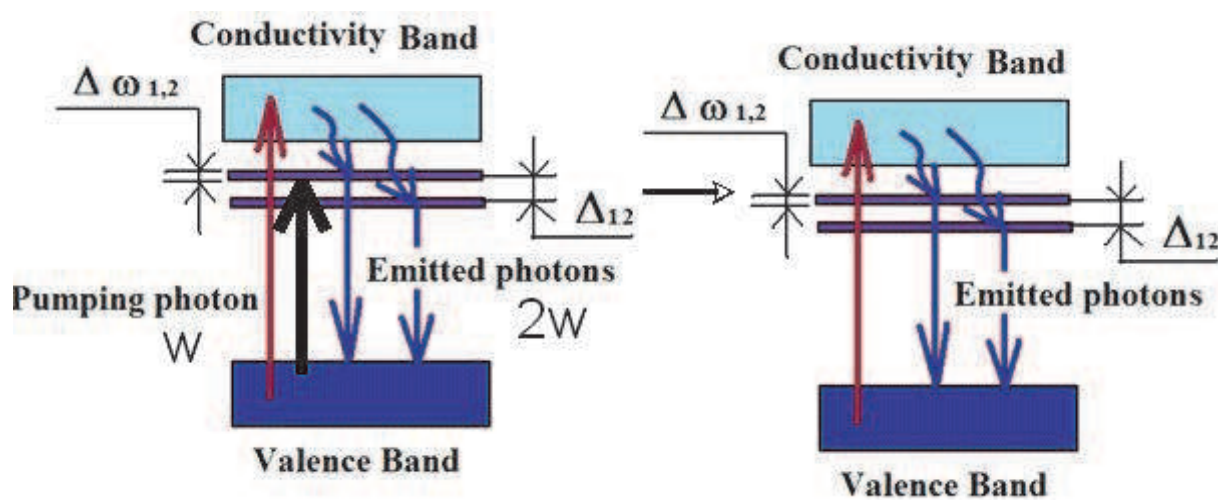


Fig. 17. The energy diagram and resonant SHG scheme by optical pumping of laser light with determined energy of pumping photon 1.63 eV (black arrow). The nonresonant excitation of carriers was illustrated by red arrow.

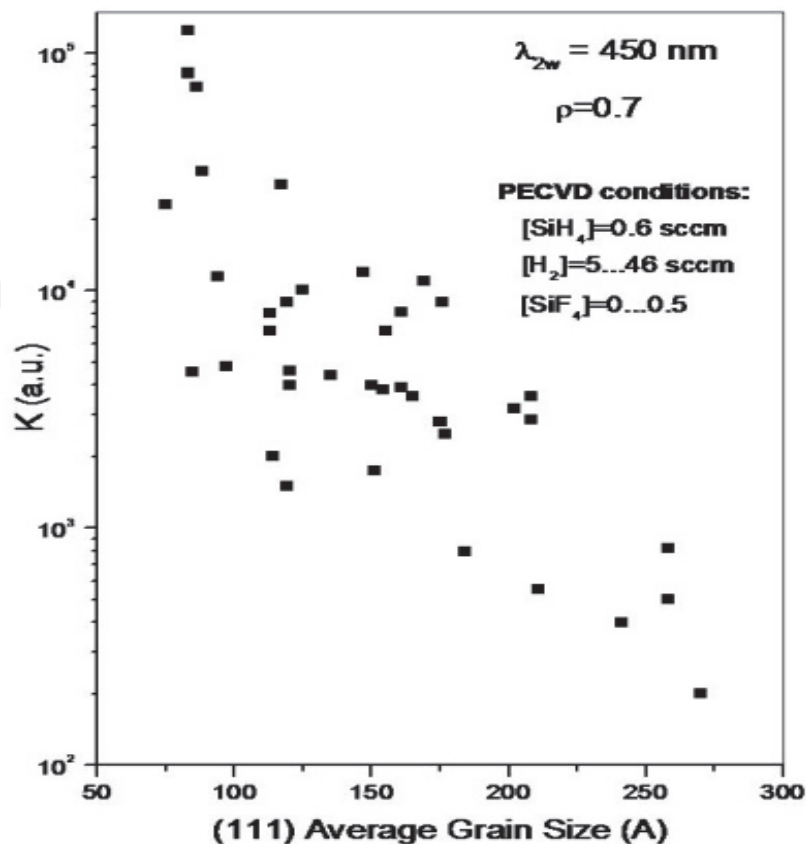


Fig. 18. SHG signals ($P_{in} \rightarrow S_{out}$) as a function of average grain sizes of nanocrystals in various silicon films deposited on glass substrates by detection the SHG radiation with wavelength 450 nm.

is normalized SHG signal, $L(2\omega, \rho)$ and $L(\omega, \rho)$ are the factors of the local field:

$$L(\omega, \rho) = \frac{\rho}{4\pi} \frac{(\epsilon_c(\omega) - \epsilon_a(\omega))}{1 + (\epsilon_c(\omega) - \epsilon_a(\omega))(\Lambda - \beta\rho)} \quad (20)$$

where ϵ_c and ϵ_a are dielectric functions of crystalline and amorphous silicon, respectively. For sphere depolarization factor Λ is equal to $1/3$, β is the Lorentz constant (for homogeneous spherical surrounding $\beta = 1/3$). For calculations the following estimated values were $\lambda_w = 900$ nm, $\lambda_{2w} = 450$ nm, $\epsilon_c'(\omega) = 13$, $\epsilon_c''(\omega) = 0.03$, $\epsilon_a'(\omega) = 12$, $\epsilon_a''(\omega) = 0.23$, $\epsilon_c'(2\omega) = 18$, $\epsilon_c''(2\omega) = 0.5$, $\epsilon_a'(2\omega) = 18$, $\epsilon_a''(2\omega) = 7.5$. It is shown on Fig. 18 that decrease in the average size of crystallites from 25 to 7.5 nm results in increasing of SHG intensity more than two orders of magnitude. Each point corresponds to one silicon film with its unique deposition conditions.

3.4 Thin nanocrystalline silicon film for nonlinear devices development

Nonlinear properties such as second-harmonic generation (SHG) were studied by means of spectroscopic technique: laser source with monochromator coupled with photo multiplied tube. Optical parametrical generator with amplifier (MOPO 730, Spectra Physics) was used to probe silicon films. The wavelength was changed in range of 450-550 nm. The diameter of laser beam on silicon film was 1 mm^2 .

Figure 14 and Fig. 15 illustrate the SHG spectra from nanocrystalline silicon films with different average grain sizes: 9.7 nm and 16.1 nm (Milovzorov et al, 2001). It is seen, that there are two spectral peaks in SHG spectra for silicon films by laser radiation $P_{in} \rightarrow P_{out}$ polarization scheme. However, in contrast to the $P_{in} \rightarrow S_{out}$ experiments (see Fig.14) with size dependent integral SHG signal there is no strict size dependence for scheme of radiation $P_{in} \rightarrow P_{out}$ (see Fig. 16) due to the negligible integrated signal.

3.5 Quantum description of microholes for SHG

Nonlinear optical semiconductor-based devices are successfully implemented in various fields of electronics as quantum electronics for SHG as fiber optics for the new Raman lasers design. Some of the structures (Pellegrini et al., 1999) such as ZnSe with microhole and Bragg reflectors $\text{Si}_3\text{N}_4/\text{SiO}_2$ generate the SHG in blue-green spectral range (460-500 nm). These conditions for SHG can be estimated as holes layer thickness $L_{cav}=360$ nm and length of coherence $l_c=1500$ nm. For silicon nanostructured films with microholes operating at 1500 nm the optical signal strictly depends on the hole geometry. SHG spectral peaks in all silicon photonic crystals can be detected at 40° and 45° for angles on incidence in the range of 700-950 nm (Dolgova et al., 2002). For nanosized holes included in nanostructured films such as shown on Fig.3 it is supposed that the inner space of holes were covered by hydrogen and oxygen atoms incorporated into silicon. These atoms terminated dangling bonds of silicon by the deposition and cancelled the further growth of crystal structure. The surface diffusion coefficient for hydrogen atom is more than for oxygen which has high electronegativity (3.44 for O and 2.1 for H). Because, the hydrogen atoms (and dangling bonds, respectively) can easily move by laser field interaction and significant dipole moments will appear. Such quantum nanoholes with defects and impurities generate additional local surface levels in electronic structure (or polaritons). The simplest possible description is coupling of exciton and photon that produces the resulted frequency value for polariton. This polariton generates SHG radiation. The frequency eigenvalues are given by (Deveaud, 2007)

$$\omega = \frac{\omega_{ex} + \omega_{ph} - i(\gamma_{ex} - \gamma_{ph})}{2} \pm \frac{1}{2} \sqrt{\Omega_R^2 + (\omega_{ex} - \omega_{ph} - i(\gamma_{ex} - \gamma_{ph}))^2}; \quad (21)$$

where ω_{ex} and ω_{ph} are exciton and nanocavity (or nano-hole) photon mode frequency, Ω_R is the Rabi frequency, γ_{ex} and γ_{ph} are, respectively, damping rates. According to the proposed model of quantum description of SHG caused by nano-sized cavities we assume that by the polariton-photon scattering SHG results in $2\omega_{laser} = \omega_{Si-O} + \omega_{ex} + \omega_s$, where the frequency is written as $\omega_s = \frac{\mu E}{\hbar}$; and $\mu = dQ$ is dipole moment of nanosized hole, d is the size of hole, Q

is charge. Figure 15 shows SHG spectra nanocrystalline silicon films with grain sizes 9.7 nm and 16 nm. The spectral peak around 3.26 eV corresponds to the Si-O oscillated bonds. The second spectral peak has random energetic position. It is assumed that its position depends on the charges distributed on film surface, particularly in man-sized holes. Accordingly, there is no observed microholes on the surface of film by using Raman mapping data (Fig.3). But for atomic-force microscopic photo it is seen the random nanosized holes. Xu proposed the method of fabrication of two-dimensional arrays of nano-holes on the silicon crystalline surface (Xu, 2004). The sharp spectral peak (see Fig. 19) reflects the high efficiency of such structures.

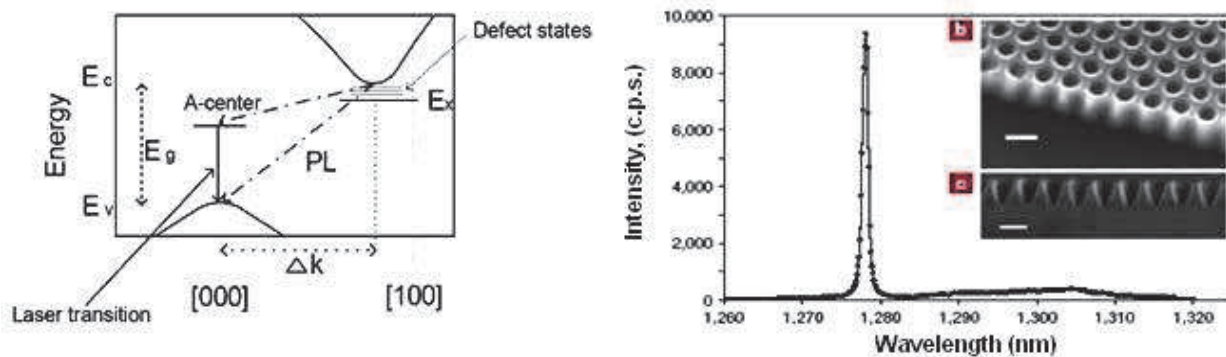


Fig. 19. Silicon energy diagram with laser transition and PL (left graph) and optical spectrum (right graph) with inserted photo of nano-holes (Xu, 2004).

3.6 Dipole moment of strained Si-O-Si

We can estimate the value of dipole moment as following:

$$\mu_{2pO-3pSi}^{Si-O-Si} = 2\sqrt{2}\pi e \int_0^{\xi} \int_0^{2\pi} \int_0^{\pi} \Psi_{3pXSi} \Psi_{3pYSi} r \Psi_{2pX-O} \Psi_{2pY-O} r^2 dr d\phi d\theta; \quad (22)$$

Usually, for Si-O-Si bridge the angle between two bonds is approximately in the range of 90-180°. The dipole moment can be estimated as $\mu_{Si-O-Si} \approx 1.4\mu_{Si-O}$ for the angle $\alpha \rightarrow 90^\circ$ between two Si-O bonds in Si-O-Si configuration. Such increasing of dipole value can be resulted by stress of film surface or even structural point defects in grain boundary of silicon nanocrystals. The stress by applied electrical field the dipole moment value for Si-O-Si bridge is defined by displacement evolution: $\mu = \mu^0 + \mu_x(t) \approx ex(t)$. We can evaluate the dipole moment by zero displacement $\mu_{Si-O-Si}^0 = 0.17D$. It is supposed, that the field-stimulated dipole moment can be varied in range of 0-1.4 D. The nonlinear susceptibility tensor is given by $\chi_{\alpha\beta\gamma} = \partial^2 P_\alpha / \partial E_\beta \partial E_\gamma$. The second-harmonic generation is forbidden for centrosymmetric crystal such as bulk silicon because the sum dipole moment is zero, but SHG is possible due to the surface breaking symmetry and quadruple terms contributions. The opposite situation is for nanostructured oxidized silicon film, the surface area for a great amount of nanocrystals is significant, and the breaking symmetry is permanent and lateral isotropic. We can use the following expressions for simplest formula of tensor such as $\alpha = N_{Si-O} / N$ and $\beta = N_{db} / N$:

$$\chi_{nc-Si}^{(2)} = \begin{pmatrix} \alpha d_{11}^o + \beta d_{11} & -\alpha d_{11}^o - \beta d_{11} & \beta d_{13} & \alpha d_{14}^o & \beta d_{15} & 0 \\ 0 & 0 & 0 & \beta d_{15} & -\alpha d_{14}^o & \alpha d_{11}^o - \beta d_{11} \\ \beta d_{31} & \beta d_{31} & \beta d_{31} & 0 & \beta d_{35} & 0 \end{pmatrix}; \quad (23)$$

There are many atoms of surface which are involved into complicated dipole moment of nanocrystals with different shapes. By decreasing the size of nanocrystal it can be observed the increasing in quantity of surface atoms and Si-O bonds which results in an appearance of charges on nanocrystal surface. Most of them are oriented according to the dominant crystal orientation (111) and placed in silicon atoms' sites. Because, there is a spectral peak (see Fig. 15) with energy position around 3.26 eV. The second spectral peaks in the Fig. 15 are related to the defect level because of there are unpaired silicon orbitals.

The spectral peak at 3.26 eV is an optical response from nanocrystal grain boundary that contains oxygen atoms incorporated in silicon as dipoles inside film. Figure 20 shows the resonant SHG response due to the $\chi^{(2)}_{zxx}$ and $\chi^{(2)}_{zyy}$ component of susceptibility tensor for silicon nanocrystals with orientation (111) and average grain size 9.7 nm. Time resolved picosecond spectroscopy was used to investigate the electronic structure of defect levels of silicon (see Fig. 5). There is a possibility to develop optoelectronic device based on polarized nanocrystalline silicon film for switching the spectral TE and TM modes of the radiation.

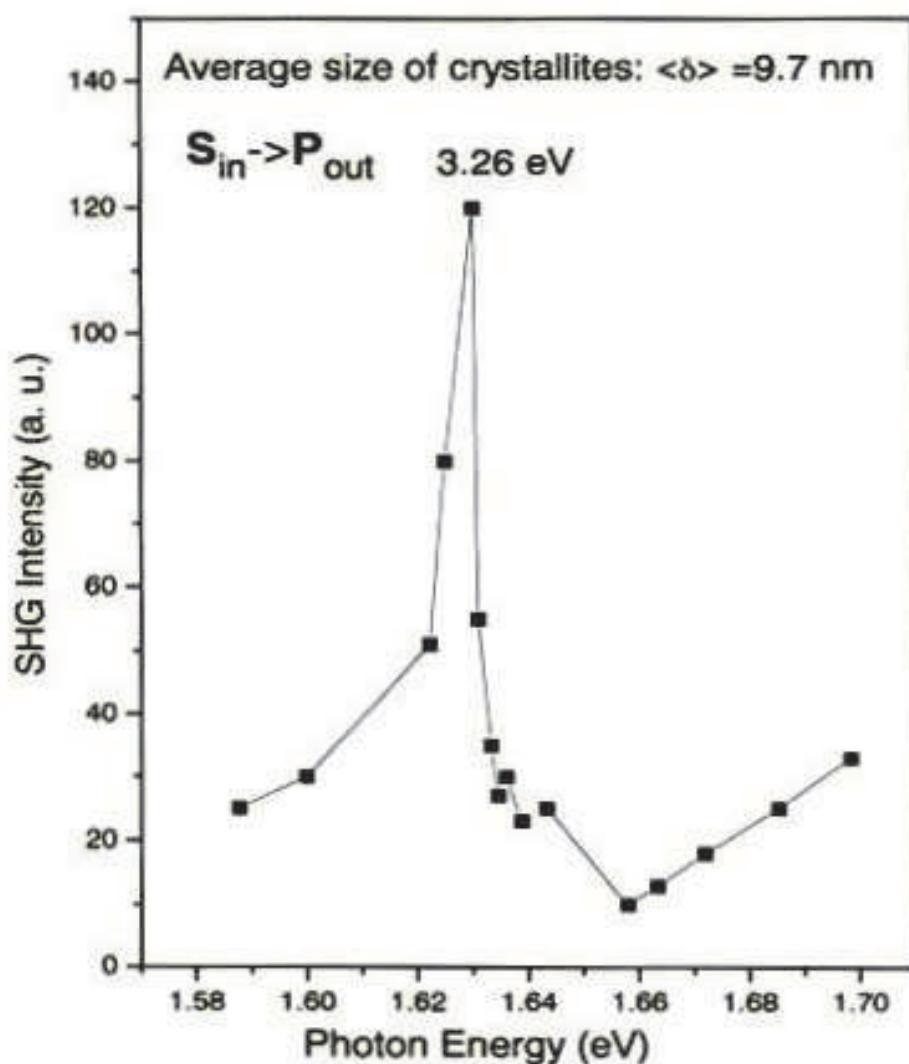


Fig. 20. Resonant SHG spectra for $\chi^{(2)}_{zxx}$ and $\chi^{(2)}_{zyy}$ component of susceptibility tensor for silicon nanocrystals with orientation (111) and average grain size 9.7 nm

3.7 Nonlinear switch parameters

The nonlinear optical semiconductor-based device is proposed. Figure 21 illustrates the scheme of second-harmonic switching. Adjusted two pairs of metal electrodes create the electric lateral field. The incident radiation has its polarization that can be transformed along the two X and Y-axis. To obtain significant SHG response it is needed to orient dipoles in silicon film. Usually, for these purposes the gold electrodes are used. Also, the rectangular

geometry with sufficient size for laser beam (from μm to mm) placing on film is popular. The film thickness is varied from the several hundredths of nm to μm . Metal electrodes are deposited by thermal evaporating by using electromagnetic inductor-based evaporator. For reorientation dipoles we need to use electrical field values sufficient for sure dipole manipulation, from one side, and comparable with laser field value, from another side. For the Ar laser radiation with power 2 mW it is used the electric field $30 \mu\text{V}/\text{nm}$. By this way, to correct the changes in dipoles' orientations by laser field is necessary for significant SHG signal detection. The polarization of film can be written as following:

$$\begin{bmatrix} P_x \\ P_y \\ P_z \end{bmatrix}^{SHG} = \epsilon_0 \chi_{nc-Si}^{(2)} \begin{bmatrix} E_x^2 \\ E_y^2 \\ E_z^2 \\ 2E_y E_z \\ 2E_x E_z \\ 2E_x E_y \end{bmatrix}; \quad (24)$$

The terms of tensor (from eq. 23) which describe silicon atoms with Si-O bonding are $\chi_{xxx}^{2w} = \alpha d_{11}^0 + \beta d_{11}$; and $\chi_{yxz}^{2w} = \alpha d_{14}^0$. The lowering of oxygen concentration ($\alpha \rightarrow 0$) in silicon film causes the elimination of related component and the view of tensor shows pure silicon surface. In addition, the P_y^{2w} component will be equal to zero. The output radiation will be polarized, too. The oxygen incorporation with silicon atoms causes the changes in χ^{2w}_{xxx} and isotropic term (χ_{yxz}^{2w}) will appear. By the $E_x=0$ the polarization components of reflected radiation from silicon film will be following

$$\begin{aligned} P_x^{2w} &= \chi_{yyy}^{2w} E_y^2 + \chi_{xzz}^{2w} E_z^2 + 2\chi_{yyz}^{2w} E_y E_z; \\ P_y^{2w} &= 2\chi_{yyz}^{2w} E_y E_z; \\ P_z^{2w} &= \chi_{zyy}^{2w} (E_y^2 + E_z^2). \end{aligned} \quad (25)$$

The components along the axis Y and Z of polarization don't depend on the Si-O bonding. However, the nonzero P_x^{2w} component contains the terms in which the Si-O dipoles are contributed. By the polarized incident radiation $E_y=0$ we will have the

$$\begin{aligned} P_x^{2w} &= \chi_{xxx}^{2w} E_x^2 + \chi_{xzz}^{2w} E_z^2 + 2\chi_{xxz}^{2w} E_x E_z; \\ P_y^{2w} &= 2\chi_{yxz}^{2w} E_x E_z; \\ P_z^{2w} &= \chi_{zxx}^{2w} (E_x^2 + E_z^2) + 2\chi_{zcx}^{2w} E_x E_z. \end{aligned} \quad (26)$$

The term that describes the oxidation of silicon with Si-O bonding is in the $\chi_{xxx}^{2w} = \alpha d_{11}^0 + \beta d_{11}$; and $\chi_{yxz}^{2w} = \alpha d_{14}^0$. The P_y^{2w} component will be equal to zero.

4.1 Light emitting devices by optical pumping

4.1.1 Light emitting devices based on photoluminescence in visible range from oxidized nanocrystalline silicon

Controlled PL from silicon nanocrystals in vertical optical cavity (Inokuma et al., 2003) with distributed Bragg reflector (DBR) was performed with deepness 800 nm corresponds to maximum yield of PL wavelength. DBR (see Fig. 22) was made by using ten periodic layers

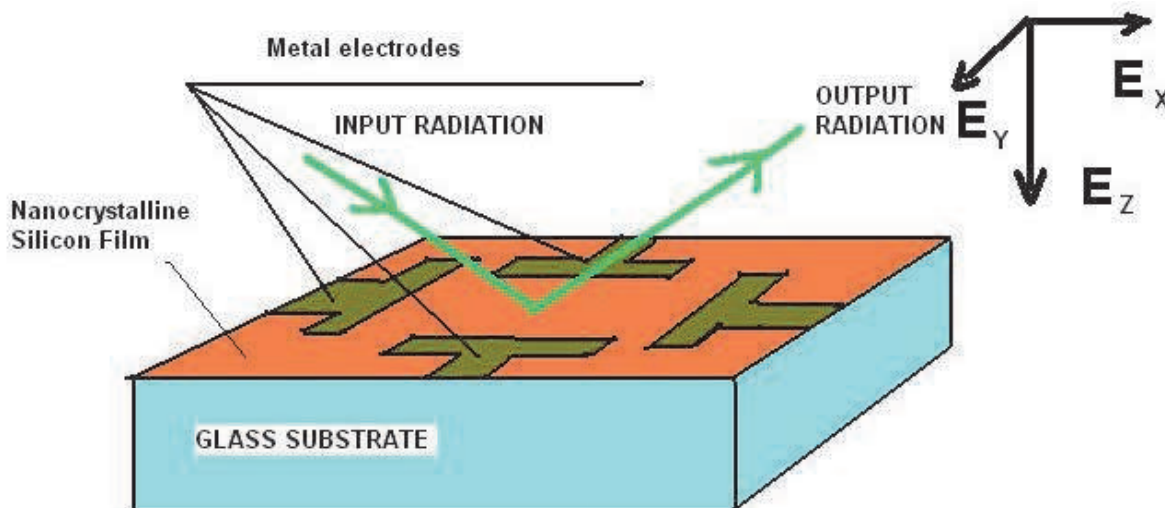


Fig. 21. Scheme of nonlinear optical semiconductor-based device.

of SiO_{1.3} and SiO_{1.8} with thickness 200 nm. Next, active layer with SiO_{1.6} has its thickness of 800 nm. This layer was served, also, as optical cavity. It was completed by using annealing to 1100°C of silicon oxide film to produce the nanocrystals. Light emitting device can surely emit at the wavelength 800 nm.

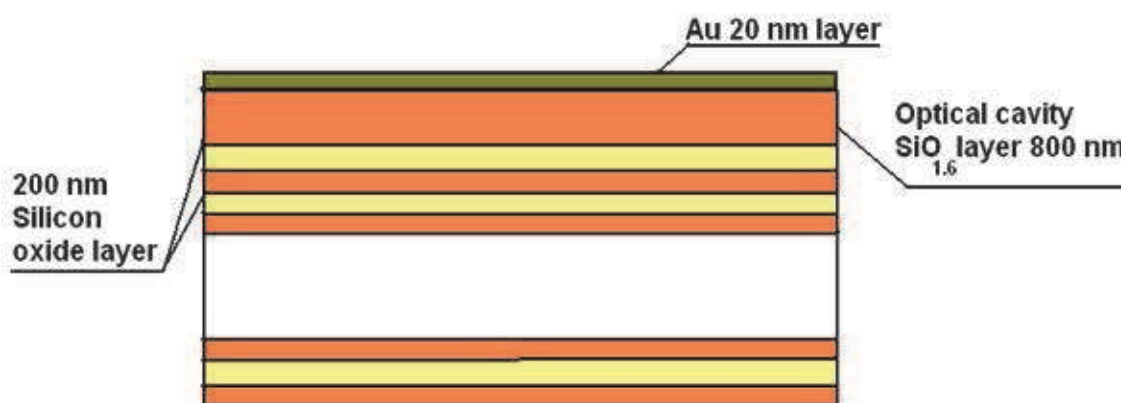


Fig. 22. Scheme of optical cavity with Au 20 nm top reflector layer and DBR (Inokuma et al., 2003).

4.1.2 Frequency-doubled resonant optically pumped vertical external-cavity laser

The process of resonance two-photon absorption can be described by means of cross-section: $W = \sigma^{(2\omega)} I^2$; where I is a fundamental radiation intensity. The cross-section of resonant two-photon absorption $\sigma^{(2\omega)}$ can be written as

$$\sigma^{(2\omega)} = \frac{512\pi^5}{h^3 c^2} \frac{\omega}{1 + 4\omega^2} \left| \sum_n \left[\frac{\langle g | \mu | n \rangle \langle n | \mu | f \rangle}{\omega_{ng} - \omega} \right] \right|^2 \quad (27)$$

By resonant two-photon absorption, usually, $\sigma^{(2\omega)}$ is approximately the same orders of magnitude as this value for one photon absorption. The energy of two-photon radiation is $E_{2\omega} = 3.26\text{eV}, (\lambda = 380\text{nm})$ eV, that corresponds to the energy of defect level (VO) inside band

gap of silicon by direct transitions. The cavity with length ℓ (see Fig. 23) is adjusted according to following requirements: $\Delta\nu = \frac{c}{2nl}$; $l = m\lambda$. Active layer that is made from nanocrystalline oxidized silicon has the thickness $d = 380$ nm. Therefore, the conditions for lasing are the following: $\exp(\gamma d)[1 - L] = 1$; $L = 1 - r_1 r_2 \exp(-\alpha(l + d))$. The resulted SHG radiation due to the two-photon resonant absorption and appearance of inverted population on the excited level. Gold electrodes (as it is shown in Fig. 23) are necessary for fine tuning the electronic structure of silicon film to eliminate the detuning between pump laser two photons and defect level position. Al mirror layer has the thickness 10 nm. By the diffraction on the silicon nanocrystals there are two tied cavities by one transition frequency. Each optical path differs from others. The estimations of frequency beats no more than 10^{12} Hz which comparable with LO phonons. From the Maxwell equation for electromagnetic media the following equations for fields, polarizations and inverted population in two interacted cavities are given by

$$\begin{aligned}\ddot{\vec{E}}_1 + \gamma \dot{\vec{E}}_1 + \omega_1^2 \vec{E}_1 &= -\gamma \dot{\vec{P}}_1 + m_1 \dot{\vec{E}}_2; \\ \ddot{\vec{E}}_2 + \gamma \dot{\vec{E}}_2 + \omega_2^2 \vec{E}_2 &= -\gamma \dot{\vec{P}}_2 + m_2 \dot{\vec{E}}_1; \\ \dot{\vec{P}}_1 + \Delta_1 \vec{P}_1 + \Omega^2 \vec{P}_1 &= \frac{-4\pi\Omega}{h} L_{\text{coeff}} \frac{|\mu_1|^2}{3} N \vec{E}_1; \\ \dot{\vec{P}}_2 + \Delta_2 \vec{P}_2 + \Omega^2 \vec{P}_2 &= \frac{-4\pi\Omega}{h} L_{\text{coeff}} \frac{|\mu_2|^2}{3} N \vec{E}_2; \\ \dot{N} + \Delta_1 (N - N_s) &= \frac{4\pi}{\Omega} \left(\dot{\vec{P}}_1 + \dot{\vec{P}}_2 \right) \left(\vec{E}_1 + \vec{E}_2 \right).\end{aligned}$$

Here, m_1, m_2 characterize the degree of interaction between the cavities, μ_1, μ_2 are matrix elements of dipole moments, L_{coeff} is Lorentz coefficient, $\gamma, \Delta_1, \Delta_2$ are the time duration of field relaxation inside cavity, broadenings of spectral lines, respectively. The solutions of system of equations can be written as harmonic functions by assumption of low changed magnitudes of field, polarization and phase values. By the way of simplification such complicated system of equations it is possible to present as the master equations for magnitudes of fields, phase and inverted population and solve them by using computer simulations:

$$\begin{aligned}\dot{E}'_1 &= E'_1 \frac{1}{2} [DgN - \gamma] + \frac{m_1}{2\omega} E'_2 \sin \Phi; \\ \dot{E}'_2 &= E'_2 \frac{1}{2} [DgN - \gamma] - \frac{m_2}{2\omega} E'_1 \sin \Phi; \\ \dot{\Phi} &= \frac{\omega_2^2 - \omega_1^2}{2\omega} + \frac{1}{2\omega} \left[m_1 \frac{E'_2}{E'_1} - m_2 \frac{E'_1}{E'_2} \right] \cos \Phi; \\ \dot{N} + \Delta_1 (N - N_s) &= -\frac{2\pi DN g \varepsilon}{h\Omega} \left((E'_1)^2 + (E'_2)^2 + 2E'_1 E'_2 \cos \Phi \right);\end{aligned}\tag{28}$$

where

$$D = \frac{4\pi\Omega}{3h\Delta_2\varepsilon} L_{coeff} |\mu|^2; \Phi = \phi_2 - \phi_1; g = \frac{\Delta_2^2}{4((\omega - \Omega)^2 + 1)}$$

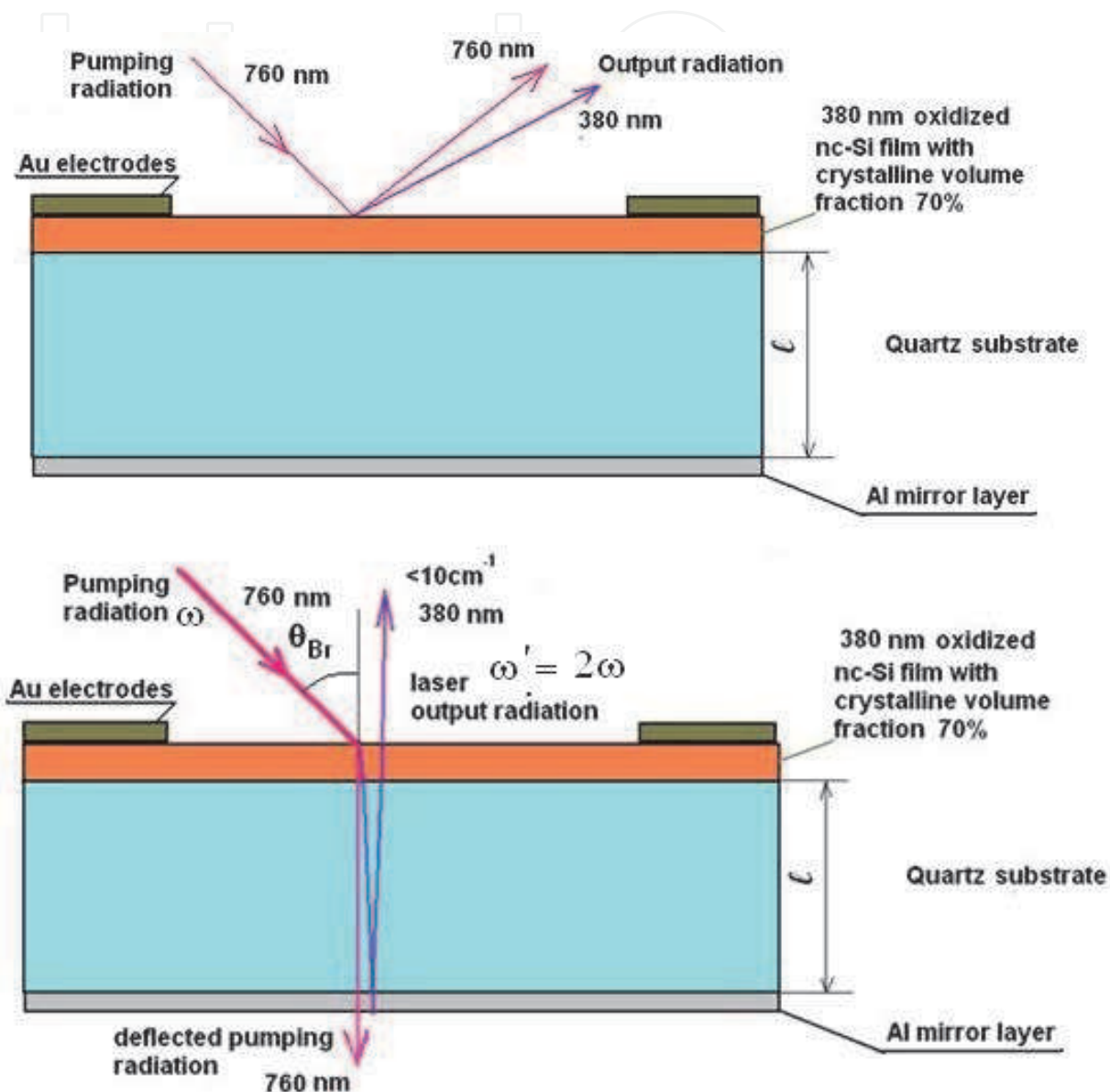


Fig. 23. Schemes of SHG switcher (upper picture) for TE mode and optical cavity and active layer serving as UV laser (down picture) with radiation at wavelength 380 nm for TM mode.

4.1.3 Damage threshold intensity

Figure 24 illustrates the SHG signal as a function of laser power with wavelength of radiation 680 nm. The maximal value of laser power reflects the damage threshold of silicon film. The intensity of SHG has the following view: $I_{SHG} = \eta_{SHG} I^2$ where $\eta_{SHG} \propto |L(2\omega, \rho)L^2(\omega, \rho)|^2 |\chi_{SHG}|^2$; $\eta_{SHG} = 0.05 \times 10^{-18} \text{ cm}^2/\text{W}$, for silicon films. By the power

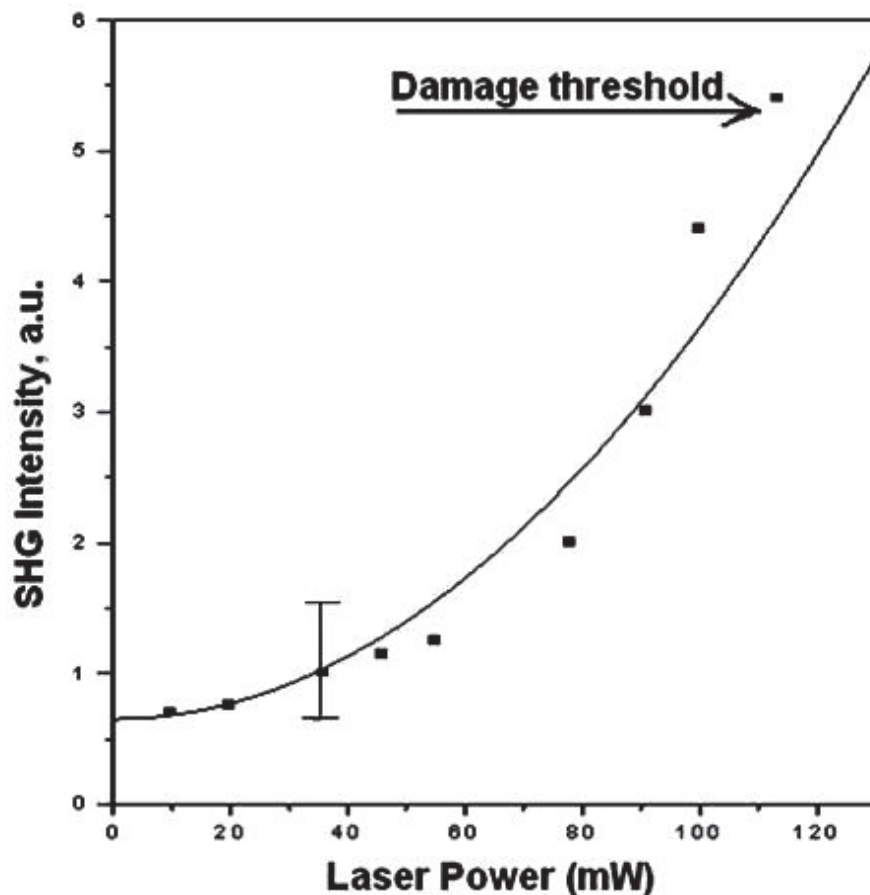


Fig. 24. SHG as a function of primary laser power for the radiation with wavelength 680 nm.

density of primary radiation 375 MW/cm^2 the intensity of SHG signal can be estimated as 12.5 mW/cm^2 poly-Si films (Milovzorov & Suzuki, 1999). The value of damage threshold intensity for p-polarized light can be represented in the form:

$$I_{\text{threshold},p} = \frac{\pi(T_{\text{melt}} - T_0)(\pi\kappa c_p \rho)^{1/2} |\epsilon'|^{3/2}}{2c\tau_p^{1/2} \epsilon''} \quad (29)$$

where κ is thermal conductivity, c_p heat capacity, T_0 is initial temperature, T_{melt} damage threshold temperature (for Si $T_{\text{melt}} = 1685 \text{ K}$), τ_p pulse of laser radiation. Using the values of $T_{\text{melt}} - T_0 = 1412 \text{ K}$, $\tau_p \approx 4 \text{ ns}$ (by $\lambda_w = 680 \text{ nm}$), $\kappa = 1.56 \times 10^7 \text{ erg/cm s deg}$, $c_p = 0.69 \times 10^7 \text{ erg/g deg}$, $\rho = 2.32 \text{ g/cm}^3$, we can estimate the damage threshold intensity $I_{\text{threshold},p} \approx 4 \times 10^8 \text{ W/cm}^2$ from (Eq.22).

4.2 Theoretical model of silicon nanocrystals by laser pumping

By this way the model of photon-assisted electron transport is proposed here. Such approach can be described in second-quantized form of operators of creating and annihilation: $H_{QE} = H + H_L + H_R$

$$H = \sum_{k=1}^N [E_{1k} c_{1k}^+ c_{1k} + E_{2k} c_{2k}^+ c_{2k} + \sum_{i,j=1}^2 (V_{ikj+1} c_{ik}^+ c_{jk+1} + h.c.) + (V_{12k} c_{1k}^+ c_{2k} + h.c.)] \quad (30)$$

where E_{1k} , E_{2k} are the energies of levels, V_{ijk+1} is matrix element of tunneling, H_R and H_L are the terms which describe the right and left branches from the system, V_{12k} is the matrix element that describes the interaction of system with laser radiation. The matrix element of tunneling depends on the time as $V_{ijk+1} = V_{ijk+1}^0 \exp(-S)$, where, according to the perturbation theory, $U = U_0 + \delta U$, $\delta U(t) = eV_{ext} + eE_l x \cos(\omega_l t)$. Here $\delta U \ll U_0$. The master equation for the creation-annihilation operators can be written in matrix form: $i\dot{C} = HC$, where the C is vector. Using block matrix 2x2 (the diagonal elements are the elements of energies of levels in two-level system, and others are tunneling matrix elements) we can write the matrix of Hamiltonian as

$$H = \begin{pmatrix} A_{11} & A_{12} & 0 \\ A_{21} & A_{22} & A_{23} \\ 0 & A_{32} & A_{33} \end{pmatrix} \tag{31}$$

where diagonal block matrix $A_{jj} = \begin{pmatrix} E_1' & 0 \\ 0 & E_2' \end{pmatrix}$ describe the energy of single quantum well interacted with electromagnetic field and eigen values of this “dressed-atom” model are following

$$E_{1,2}' = \frac{E_1 + E_2}{2} \pm \sqrt{\frac{(E_2 - E_1)^2}{4} - V_{12}V_{21}} \tag{32}$$

The non-diagonal block matrix $A_{ijk-1} = \begin{pmatrix} V'_{ikik-1} & 0 \\ 0 & V'_{jkjk-1} \end{pmatrix}$,

$$V'_{ijk-1} = \frac{V_{ikik-1} + V_{jkjk-1}}{2} \pm \sqrt{\frac{(V_{ikik-1} - V_{jkjk-1})^2}{4} - V_{ikj-1}V_{jkik-1}}$$

The solution of differential equation

$$i\dot{C}_k = \hat{H} C_k \tag{33}$$

and $C_k(t) = C_k(0) \exp\left(-i \int_0^t \hat{A}_{22} d\tau\right)$. The $C_{k+1}(t) = C_{k+1}(0) \exp\left(-i \int_0^t \hat{A}_{33} d\tau\right)$ is obtained according to

the same procedure. By this way the resulted matrix has the eigen values which correspond to the energies for interacted terms with indexes k and $k+1$. Matrix tunneling element is possible to combine of two multiplied term. Each of them explains the order 1 and 2 of perturbation energy for tunneling process through the potential barrier between quantum wells.

$$V_{ijk+1} = V_{ijk+1}^0 \exp\left(-\frac{2}{\hbar} \int_0^d \sqrt{2m(U_0 - E)} dx\right) \exp\left(\frac{1}{\hbar} \int_0^d \frac{m\delta U dx}{\sqrt{2m(U_0 - E)}}\right). \tag{34}$$

It can be used as $V_{ikj_{k+1}} = V_{ikj_{k+1}}^0 F(t)$; where $F(t) = \exp(Z \cos(\omega t))$ and parameter of field-system interaction:

$$Z = \frac{1}{\hbar\sqrt{2}} \frac{\sqrt{md^2 e E_1}}{\sqrt{U_0 - E}}. \quad (35)$$

$$n_{2k}(t) = c_{2k}^+(t)c_{2k}(t); \quad (36)$$

$$c_{2k}(t) = c_{2k}^0 \exp\left(-i \int_0^t \left[E_{2k} + \frac{\Delta_{12}(t')}{\hbar\omega}\right] dt'\right) \exp\left(i \int_0^t \frac{\Delta_{2k2k-1}(t')}{E_{2k-1} + \frac{\Delta_{12}(t')}{\hbar\omega}} dt'\right); \quad (37)$$

For upper level population it can be transformed into following expression:

$$n_{2k}(t) \cong n_{2k}^0 \left(1 + \frac{8\pi\Delta_{2k2k-1}}{\hbar\omega(E_{2k} + \frac{\Delta_{12}(t')}{\hbar\omega})} \sum_m J_m(Z) J_m(-Z) K_{2m}(-2Z_2)\right); \quad (38)$$

The saturated gain (Verdeyen, 1995) of a laser oscillator is stated as

$$G^2 = \frac{1}{R_1 R_2} \left[1 - n_2 c \sigma \hbar \nu \frac{(1 - R_1 R_2)}{P_{out}}\right].$$

It is assumed, that for the scheme which is shown in Fig 23 the laser technical features

are following: reflection of Al mirror and silicon film is $R_1 = 0.99, R_2 = 0.57$, respectively, frequency of laser generation by two-photon pumping mode: $\nu = 7.510^{14} \text{ Hz}$. The value σ is stimulated emission cross section that can be evaluated as 10^{12} cm^2 , but output laser power $P_{out} \approx 17 \text{ mW}$. Accordingly, $G^2 \ll 1$, because of there is no saturation of upper level population. The losses of radiation inside cavity are managed by bias voltage applied to electrodes as shown in Fig.23. The quality factor of the cavity should be more than 10^3 . In addition, the unsaturated gain and inverted population are linear related as $G = \sigma(n_{2k} - n_{1k})$. Evolution of upper-level population of two-level system by laser pumping is illustrated in Fig. 25. For high carrier diffusion values and small laser field (see Fig. 25 a) and b)) the saturation mode of upper-level populations can be surely observed. By changing in photon energy of laser radiation and electron level detuning, the difference between the electron energy and energy position of level, the Z parameter there is a several modes in population dynamics correspond to the ordinary laser active media modes.

5. Conclusions

Optical spectral characteristics for nanocrystalline silicon films are investigated for their application in optoelectronic device manufacturing. Different optoelectronic devices based on nanocrystalline silicon films such as acoustoelectrical optical mode switcher for laser radiation, nonlinear optical switcher, and frequency-doubled resonant optically pumped vertical external-cavity laser is proposed. There is a significant yield from the using nanocrystalline silicon films in device implementation for optoelectronic. Their application is wide spread and became broader than before by each year. Frequency-doubled, optically

pumped vertical external-cavity surface-emitting lasers (VECSEL) have numerous applications as for waveguiding and flat panel displays. In recent years the fiber laser have grown in power as on their fundamental frequencies as in SHG yields.

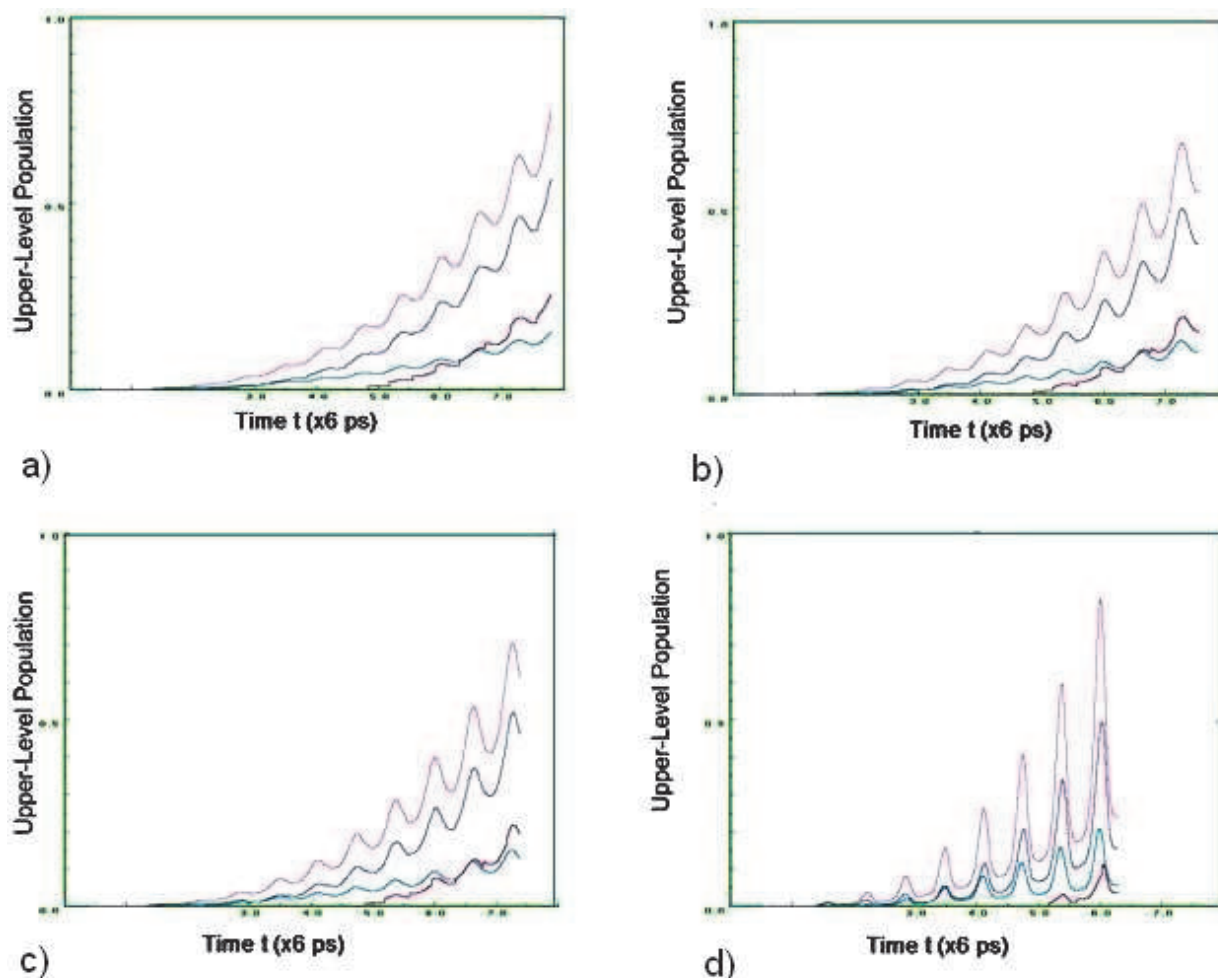


Fig. 25. Evolution of upper-level population for system with index $k=38$ by the parameters: a) $Z=0.3$; $\Omega=90$ GHz; b) $Z=0.5$, $\Omega=150$ GHz; c) $Z=0.6$, $\Omega=180$ GHz;d) $Z=1$, $\Omega=0.6$ THz.

The nonlinear optical processing the signal often depends on the variation in refraction of index which changes the speed of travelling through the fibre and these results in an error signal appearance. It is dramatic by transmission the signal up to 1000 km and more. There are problems which signal degradation: amplification of spontaneous emission, four-wave mixing, self-phase mixing and cross-phase mixing. All of them results in degrading the signal to noise ratio (SNR). For 10 Gbit/s this ratio 100:1, or 20 dB (Livas, 2002). Using two mode laser with two interacted cavities can be easily used to prihibit high losses and prevent the signal changes due to refraction index deviation. Multiple optical beams in optical network pass through a large number of wavelength switchers which consist of multiplexer, demultiplexer, optical cross connects, optical amplifiers. Using the Raman amplifiers based on stimulated Raman scattering effect is, also, very effective because there is a possibility in using any type of transmission fiber.

Polarization is caused by the interaction of radiation with the molecules of fiber. The degree of polarization depends on the temperature and stress conditions, such as stretching and

bending modes of silica molecules of the fiber. If polarization of fiber is changing the polarization dispersion is increases and polarization-dependent losses increase, too. Fiber amplifier (FA) cuts the determined frequency from the others as filter by its amplifying. By using the FA device to input signal the SNR is affected, by using it to output signal the amplitude is dramatically increasing. To prevent the losses by modal dispersion is possible to change mode and use another single mode fiber. The laser systems with interacted cavities can be used to change the frequency modes from the one to another by efficient transfusion of laser energy. Accordingly, by using conversation law for both photons of modes which are closed each to other it is possible to determine the signal from new frequency mode. Therefore, the further investigations open great possibilities to make new optoelectronic devices fore speed data transforming and data recognition in optical networking

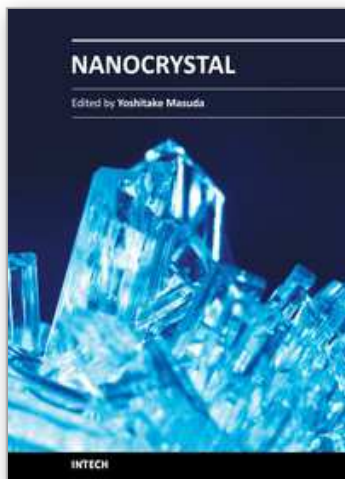
6. References:

- Chabal, Y., Raghavachari, K., Zhang, X., Garfunkel, E., Silanone on Si (100): intermediate for initial silicon oxidation, *Physical Review B*, 66 (2002) 161315-1-4. ISSN 0163-1829.
- Chatterjee, A., Iwasaki, T., Ebina, T., Structural and energetic changes of Si (100) surface with fluorine in presence of water – a density functional study, *International Journal of Molecular Sciences*, 2 (2001) 40-56, ISSN 1422-0067.
- Corbett, J., Watkins, G., Chrenko, R., McDonalds, R., Defects in Irradiated Silicon: Infrared Absorption of the Si- A center, *Physical Review*, v.121, n4, (1961) 1015-1022 ISSN 0163-1829.; Corbett, J., Watkins, G., McDonalds, R., New oxygen infrared bands in annealed irradiated silicon, *Physical Review*, v.135, N5A, (1964) A1381-A1385. ISSN 0163-1829.
- Delerue C., Allan, G., Lanoo, M., Theoretical aspects of the luminescence of porous silicon, *Physical Review B*, V.48, N.15, 15 October 1993, 11024-11036. ISSN 0163-1829.
- Deveaud, B., *The physics of semiconductor microcavities*, Wiley-VCH Verlag GmbH & Co., Wiendheim, 2007, p. 7.
- Dolgova, T., Maidikovski, M., Martemyanov, M., Fedyanin, A., Aktsipetrov, O., Marowsky, G., Yakovlev, V., Mattei, M., Giant microcavity enhancement of second-harmonic generation in all-silicon photonic crystals, *Applied Physics Letters*, 81, 2725-2727 (2002) ISSN 0003-6951.
- Durr, M., Hofer, U., Dissociative adsorption of molecular hydrogen on silicon surface, *Surface Science Reports*, 61 (2006) pp.465-526.
- Feuer, P., Electronic States in Crystals under Large Over-All Perturbations, *Physics Review*, v.88, n.1, (1952) 92-100. ISSN 0163-1829, ISSN 0163-1829.
- Han, D., Yue, G., Lorentzen, J., Lin, J., Habuchi, H., Wang, Q., Optical and electronic properties of microcrystalline silicon as a function of microcrystallinity, *Journal of Applied Physics*, 87, 1882 (2000)ISSN0021-8979; Han, D., Lorentzen, J., Weinberg-Wolf, J., MCNeil, L., Raman study of thin films of amorphous-to-microcrystalline silicon prepared by hot-wire chemical vapor deposition, *Journal of Applied Physics*, 94, 2930 (2003) ISSN0021-8979.

- Inokuma, T., Kurata, Y., and Hasegawa, S., Controlled photoluminescence from silicon nanocrystals in a vertical optical cavity with distributed Bragg reflectors, *Physica Status Solidi (c)*, 0, N4(2003) 1258-1261. ISSN 1610-1634.
- Kahan, V., High frequency hopping transport in solids and dielectric transparency in compensated semiconductors, *JETP*, 117, (2000) 452-456.
- King, R., Mastrykov, V., Schaefer, H., The electron affinities of the silicon fluorides SiF_n (n=1-5), *Journal of Chemical Physics*, 105, (1996) 6880-6886. ISSN 0021-9606.
- Klein, W., Cook, B., Unified approach to ultrasonic light diffraction, *IEEE Transaction*, SU-14, N3 (1967) 123134. ISSN 0018-9383.
- Lanoo, M., Allan, G., A cluster plus effective tight-binding study of SiO_x systems, *Solid State Communications*, 28 (1978) 733-739. ISSN 0038-1098.
- Livas, J., Conditioning squeezes the best out of signals, *Lightwave Europe*, October 2002, 18-20 ISSN 1447-5069.
- Matsuda, A., Growth mechanism of microcrystalline silicon obtained from reactive plasmas, *Thin Solid Films*, 337 (1999) 1-6 ISSN 0040-6090; Matsuda, A., Microcrystalline silicon. Growth and device application, *Journal of Non-Crystalline Solids*, 338-340 (2004) 1-12. ISSN 0022-3093.
- Milovzorov, D., Inokuma, T., Kurata, Y., Hasegawa, S., Relationship between structural and optical properties in polycrystalline silicon films prepared at low temperature by PECVD, *Journal of Electrochemical Society*, 145, (1998) 3615-3620; Milovzorov, D., and Suzuki, T., Size-dependent second harmonic generation of nanocrystals prepared by plasma-enhanced chemical vapor deposition, *Applied Physics Letters*, 75, 4103-4105 (1999) ISSN 0003-6951.; Milovzorov, D., Ali, A., Inokuma, T., Kurata, Y., Suzuki, T., and Hasegawa, S., Optical properties of silicon nanocrystallites in polycrystalline silicon films prepared at low temperature by plasma-enhanced chemical vapor deposition, *Thin Solid Films*, 382, 53-55 (2001) ISSN 0040-6090; Milovzorov, D., Electronic structure of nanocrystalline silicon and oxidized silicon surfaces, *Electrochemical and Solid State Letters*, 4(7), 2001, G61-63 ISSN 0013-4651; Milovzorov, D., Point defects in amorphous and nanocrystalline fluorinated silicon films, *Journal of Materials Science and Engineering with Advanced Technology*, v.2, n.1, (2010) 41-59. ISSN 0976-1446.
- Pellegrini, V., Colombelli, R., Carusotto, I., Beltram, F., Rubini, S., Lantier, R., Franciosi, A., Vinegoni, C., Pavesi, L., Resonant second harmonic generation in ZnSe bulk microcavity, *Applied Physics Letters*, 74, 1945-1947 (1999). ISSN 0003-6951.
- Rotter, M., Wixfirth, A., Rulle, W., Bernklau, D., Riechert, H., Giant acoustoelectric effect in GaAs/liNbO₃ hybrids, *Applied Physics Letters*, 73 (1998) 2128-2130. ISSN 0003-6951.
- Shklyae, A., Aono, M., Suzuki, T., Thermally enhanced second-harmonic generation, *Surface Science*, 423, 61 (1999) ISSN 0039-6028.
- Tsu, D., Chao, B., Ovchinsky, S., Jones, S., Heterogeneity in hydrogenated silicon: Evidence for intermediately ordered chainlike objects, *Physical Review B*, 63, 125338 (2001). ISSN 0163-1829.
- Verdeyen, J., *Laser electronics*, Prentice Hall, London, 1995, p. 150. ISBN 0-13-101668-7.

- Wang, J., Zou, B., El-Sayed, M., Comparison between the polarized Fourier-transform infrared spectra of aged porous silicon and amorphous silicon dioxide films on Si(100) surface, *Journal of Molecular Structure*, 508 (1999) 87-96. ISSN 0022-2860.
- Weinreich, G., Sanders, T., White, H., Acoustoelectric effect in n-type Germanium, *Physical Review*, 114 (1959) 33-44. ISSN 0163-1829.
- Xu, J., Div Engineering, Directly Pumped Crystalline Silicon Laser an impossible possibility, Brown University, Providence, RI 02912, 213-215, ISBN:1-4244-0096-1, INSPEC Accession Number:9274227.
- Yu P., Cardona M., *Fundamentals of semiconductors, Physics and Materials Properties*, Springer, Berlin, 1996, p.207. ISBN3-540-61461-3.

IntechOpen



Nanocrystal

Edited by Dr. Yoshitake Masuda

ISBN 978-953-307-199-2

Hard cover, 494 pages

Publisher InTech

Published online 28, June, 2011

Published in print edition June, 2011

We focused on cutting-edge science and technology of Nanocrystals in this book. “Nanocrystal” is expected to lead to the creation of new materials with revolutionary properties and functions. It will open up fresh possibilities for the solution to the environmental problems and energy problems. We wish that this book contributes to bequeath a beautiful environment and valuable resources to subsequent generations.

How to reference

In order to correctly reference this scholarly work, feel free to copy and paste the following:

Dmitry E. Milovzorov (2011). Nonlinear Optoelectronic Devices Based on Nanocrystalline Silicon Films: Acoustoelectrical Switches for Optical Modes, Nonlinear Optical Switches and Lasers, Nanocrystal, Dr. Yoshitake Masuda (Ed.), ISBN: 978-953-307-199-2, InTech, Available from:
<http://www.intechopen.com/books/nanocrystal/nonlinear-optoelectronic-devices-based-on-nanocrystalline-silicon-films-acoustoelectrical-switches-f>

INTECH
open science | open minds

InTech Europe

University Campus STeP Ri
Slavka Krautzeka 83/A
51000 Rijeka, Croatia
Phone: +385 (51) 770 447
Fax: +385 (51) 686 166
www.intechopen.com

InTech China

Unit 405, Office Block, Hotel Equatorial Shanghai
No.65, Yan An Road (West), Shanghai, 200040, China
中国上海市延安西路65号上海国际贵都大饭店办公楼405单元
Phone: +86-21-62489820
Fax: +86-21-62489821

© 2011 The Author(s). Licensee IntechOpen. This chapter is distributed under the terms of the [Creative Commons Attribution-NonCommercial-ShareAlike-3.0 License](#), which permits use, distribution and reproduction for non-commercial purposes, provided the original is properly cited and derivative works building on this content are distributed under the same license.

IntechOpen

IntechOpen